NASA TECHNICAL NOTE

NASA TN D-2846

NASA TN D-2846

EFFECTS OF LEADING-EDGE BLUNTNESS ON PRESSURE AND HEAT-TRANSFER MEASUREMENTS OVER A FLAT PLATE AT A MACH NUMBER OF 20

by William D. Harvey

Langley Research Center
Langley Station, Hampton, Va.

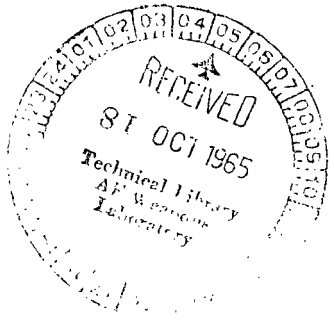

NATIONAL AERONAUTICS AND SPACE ADMINISTRATION • WASHINGTON, D. C. • OCTOBER 1965

NASA TN D-2846

EFFECTS OF LEADING-EDGE BLUNTNESS ON PRESSURE AND HEAT-TRANSFER MEASUREMENTS OVER A FLAT PLATE AT A MACH NUMBER OF 20

By William D. Harvey

Langley Research Center
Langley Station, Hampton, Va.

NATIONAL AERONAUTICS AND SPACE ADMINISTRATION

For sale by the Clearinghouse for Federal Scientific and Technical Information
Springfield, Virginia 22151 – Price $2.00

EFFECTS OF LEADING-EDGE BLUNTNESS ON PRESSURE AND HEAT-TRANSFER MEASUREMENTS OVER A FLAT PLATE AT A MACH NUMBER OF 20

By William D. Harvey
Langley Research Center

SUMMARY

An experimental investigation has been conducted to study the effects of viscous interaction and leading-edge bluntness on flat-plate pressures and heat-transfer coefficients at a Mach number of approximately 20. The investigation was conducted at a nominal stagnation temperature and pressure of about 4000° R and 10 000 pounds per square inch for a free-stream Reynolds number per foot of about 0.46×10^6.

The pressure data for the sharp leading-edge flat plate indicated a region of transition between the free molecule flow and continuum flow regions near the leading edge. Experimental results from the blunt leading-edge configurations were in agreement with those from the linear addition of inviscid and viscous effects. The blast-wave theory gave good approximations of the shock shapes of the blunt leading-edge configuration. The boundary-layer growth measured from schlieren photographs of the sharp plate gave fair agreement when compared with the hypersonic boundary-layer theory.

INTRODUCTION

There is continuing interest in low-density hypersonic flow over simple lifting shapes, such as flat plates, to study the effects of leading-edge bluntness and viscous-layer thickness on the distributions of pressure and heat-transfer rates over the plates. A number of theoretical and experimental investigations have been made to study these effects. Most of these investigations consider extremely blunt leading edges for bluntness effects or extremely sharp leading edges for boundary-layer—shock-wave interaction effects. The blast-wave theory has been used to predict the dominant bluntness effects with a fair amount of success (refs. 1 to 6), although a number of shortcomings of the blast-wave analogy are shown in references 7 and 8. The well-established weak and strong interaction theories have been used extensively to predict the continuum-flow region of the dominant boundary-layer displacement effects on the sharp leading-edge flat plate (refs. 9 to 21). At the present time, no theory adequately predicts the transition region between continuum flow and

free molecule flow near the leading edge of the plate; however, some data have been presented which include slip flow effects. (See for instance, refs. 22 to 24).

Several experimental investigations have been made to study hypersonic flow over flat plates with blunt leading edges (refs. 25 to 30). Some of these studies were conducted with adiabatic wall conditions for which the boundary-layer displacement effects are considerably larger than those anticipated for cold-wall tests considered in hypersonic-flow phenomena (refs. 25 and 26). Since the investigations often did not include both pressure and heat-transfer measurements, the analysis of the experimental data was limited.

The purposes of the present investigation were to measure the surface-pressure distribution and the heat-transfer-rate distribution simultaneously and to obtain shock-wave shapes from schlieren pictures for low-density hypersonic flow over sharp and blunt leading-edge configurations. This investigation was made in the Langley hotshot tunnel with nitrogen at a nominal free-stream Mach number of 20, a nominal Reynolds number per foot of 0.46×10^6, and a stagnation temperature of 4000° R; the corresponding ratios of wall temperature to stagnation temperature were approximately 0.13. The plates were alined with the stream at angles of attack and yaw of 0°. The variation in leading-edge bluntness from 0.0003 inch to 0.080 inch yielded Reynolds numbers based on leading-edge thickness from approximately 11.5 to 3060.

Shock shapes were determined from schlieren photographs, and detailed surface heat-transfer and pressure measurements were made. Correlation of the experimental data was made in terms of local similarity. Also, a comparison of the extended viscous similitude for bluntness was made along with a discussion of data and theory agreement.

SYMBOLS

A, B, D coefficients in equations for the zero-order strong-interaction theory (from ref. 16)

C_D nose drag coefficient

C_w viscosity-temperature ratio, $\mu_w T_\infty / \mu_\infty T_w$

C' viscosity-temperature ratio based on T' method, $\mu'_\infty T_\infty / \mu_\infty T'_\infty$

c specific heat of calorimeter sensing disk material, Btu/lb-$^\circ$F

$c_{p,\infty}$ free-stream specific heat at constant pressure

E electromotive force, volts

$G = f(T_w, T_r, \gamma, M_\infty)$ (from ref. 21)

$\bar{h}$	local heat-transfer coefficient without pressure gradient, $(dp/dx = 0)$
h	local heat-transfer coefficient with pressure gradient included $(dp/dx \neq 0)$
K_3, K_4	coefficients defined by reference 16
k	thermocouple gage-calibration constant, millivolts/^{o}F
M_∞	free-stream Mach number
m	mass, pounds
$N_{Pr,\infty}$	Prandtl number at free-stream static temperature
$N_{St,\infty}$	Stanton number including pressure gradient effect, based on free-stream properties, $\frac{h}{c_{p,\infty}\rho_\infty V_\infty}$
n	exponent in equation for variation of pressure with x, $p \propto x^n$, also the slope of the power-law curve
p	pressure, lb/sq in.
p_w	wall pressure, lb/sq in.
p_∞	free-stream pressure, lb/sq in.
q	heat content, Btu/sq ft
$\dot{q}$	local heat-transfer rate, $dq/d\tau$, Btu/ft^2-sec
R_∞	free-stream Reynolds number per foot
$R_{\infty,x}$	free-stream Reynolds number with x as characteristic length, $\frac{\rho_\infty V_\infty x}{\mu_\infty}$
R_t	Reynolds number based on leading-edge thickness
r	radius of calorimeter disk
S	area, sq in.
T	temperature, ^{o}R
T_{arc}	calculated arc chamber temperature, ^{o}R

T_r	recovery temperature, ^{o}R
T_w	wall temperature, ^{o}R
T_t	stagnation temperature behind normal shock, ^{o}R
T_∞	free-stream static temperature, ^{o}R
T'_∞	temperature evaluated by T' method (ref. 31)
t	thickness, inch
V	volume, cu in.
V_∞	free-stream velocity, ft/sec
x	distance along plate surface
y	spanwise distance on plate from model center line
z_s	vertical distance from origin (center line through model leading-edge thickness, t_{le}) to shock wave (See sketch A)
z_δ	vertical distance from plate surface to outer edge of visible boundary layer (See sketch A)
α	angle of attack, degrees
γ	ratio of specific heats
$\overline{\chi}_\infty$	hypersonic viscous parameter, $\frac{M_\infty^3\sqrt{C_w}}{\sqrt{R_{\infty,x}}}$
ρ	sensing-material density, lb/ft^3
ρ_{arc}	arc chamber density, atm
ρ_∞	free-stream density, lb/ft^3
μ_∞, μ_w	free-stream viscosity; viscosity at the wall
τ	time, sec
ϵ	correction factor in equation (5)
ψ	angle of yaw, deg

Subscripts:

c	calorimeter disk
le	leading edge

APPARATUS AND TESTS

Tunnel and Test Conditions

The present investigation was conducted in the Langley hotshot tunnel. This tunnel is similar to other hotshot facilities in that a high-energy arc is discharged within an arc chamber to heat and pressurize the test gas. Upon rupture of a diaphragm upstream of the nozzle throat, the nitrogen expands through a conical nozzle and test section into the vacuum reservoir. A detailed description of the tunnel can be found in reference 32. The arc chamber used in the present tests is the coaxial electrode arrangement described in appendix A of reference 32 without the magnetic coil. The present investigation was made at a nominal Mach number of 20, and arc chamber temperatures and pressures of approximately 4000° R and 10 000 pounds per square inch with nitrogen as the test medium.

During each test, the arc chamber pressure and test-section pitot pressure were measured and recorded. Two transducers for each measurement were employed and relatively good agreement (±4 percent) existed between the two transducers for each case. Calibrations in the anticipated pressure range for the particular test were made on each transducer beforehand.

Schlieren Apparatus

The schlieren system employed was a conventional horizontal off-axis single-pass type with 8-foot-focal-length 12-inch-diameter parabolic mirrors. The light source was a mercury arc lamp designed for either continuous or short-duration arc service. The short-duration arc light was programed at a preselected time for each test of the present investigation. Schlieren photographs were obtained on 4-inch by 5-inch film plates. Model roll and yaw were carefully adjusted to match the upper rays in the schlieren beam. The angle of attack was set with an inclinometer and was equal to zero for all configurations.

Model

The flat-plate model employed in the investigation is shown in figure 1(a). For the tunnel tests, the screw holes were filled. Figure 1(b) is a photograph of the underside of the instrumented surface and shows the pressure orifices and reference manifold. The pressure orifice tubes are shown without pressure transducers. Thermocouples are in place. The large cylinder with small tubes

protruding outwardly is the reference pressure manifold common for all transducers.

Figure 2 is a schematic drawing of the model and shows the pertinent details of the model construction and instrumented surface. Table I gives the location of the instrumentation. The model housing and sting are made of aluminum except for the instrumented plate surface which is made of stainless steel and is discussed subsequently in more detail. There are four leading-edge pieces semicylindrical in shape and interchangeable. Leading-edge thicknesses are 0.0003 inch, 0.015 inch, 0.030 inch, and 0.080 inch. Each leading-edge piece was measured with a microscope and the average thickness across the span of the model was determined with a ±0.0001-inch variation.

Heat-Transfer Gages

Heat-transfer rates of 1 to 10 Btu/ft^2-sec were expected during the present investigation with tunnel test times of about 0.100 second. In order to develop a gage that would record a nearly instantaneous surface-temperature change with time and within a very small error range, it was necessary to consider the following equation that expresses the quantity of heat contained by any body:

$$q = \frac{mcT}{S} \tag{1}$$

The rate of heat transfer to the body is given by

$$\dot{q} = \frac{dq}{d\tau} \tag{2}$$

Therefore, by differentiation and substitution of equation (1) into equation (2)

$$\dot{q} = \frac{mc}{S}\frac{dT}{d\tau} \tag{3}$$

where $m = \rho V$. For a disk $V = \pi r^2 t_c$ and $S = \pi r^2$. Substituting these equivalents into equation (3) yields

$$\dot{q} = \frac{mc}{S}\frac{dT}{d\tau} = \frac{\rho Vc}{S}\frac{dT}{d\tau} = \rho c t_c \frac{dT}{d\tau} \tag{4}$$

The change in the electromotive force in a thermocouple may be expressed as

$$dE = k\,dT$$

where k is a constant equal to the change in millivolts per degree Fahrenheit for a particular thermocouple. By substitution of $dE = k\,dT$ into equation (4), the following expression is obtained

$$\dot{q} = \frac{\rho c t_c}{k} \frac{dE}{d\tau}$$

Since k, ρ, and c are essentially constant for a particular choice of material, only the thickness t_c need be varied to adjust the sensitivity. Thus by reducing the thickness for a given thermoelement, the sensitivity is increased.

In constructing a calorimeter thermocouple gage for making the desired heating-rate measurements, the following factors were considered:

(1) The calorimeter was constructed so that the anticipated temperature rise would not exceed that of the working limits of the sensing material, bonding material, or support structure.

(2) The ratio of sensing-disk radius to thickness was made large to prevent heat losses radially outward from the material sensing area.

(3) The calorimeter needed sufficient sensitivity to produce an electrical signal which could be recorded with accuracy.

The heat-transfer gage unit was constructed at the Langley Research Center. A support plate was made of steel and was initially machined and ground on one side. Then 20 holes for pressure-orifice tubes (0.060-inch-diameter) and 21 0.25-inch-diameter holes for thermocouples were drilled at specified locations. A 0.001-inch-thick bonding material similar to double-backed tape was used to attach the 0.002-inch-thick 302 stainless-steel sheet to the support plate. This bonding resulted in a smooth uniform thin-skin surface, which served as a calorimeter-type heat-transfer gage at each of the 0.25-inch hole locations. Chromel-alumel thermocouple wires (0.001-inch diameter) were then resistance-welded on to the back side of the thin skin as near the center of the disks as possible. The wires were limited to 1/4 inch in length to minimize resistance. Copper lead wires of much larger diameter were joined to the 0.001-inch-diameter thermocouple wire which served as the cold junction for each gage.

Calibration of the gages was made by applying a known electromotive force to each thermocouple circuit including the readout equipment. The variation of the deflection in inches with millivolts was recorded for each gage prior to a test. Since the sensitivity was greatly increased by reducing the calorimeter thickness, it was found that with the proper galvanometer selection, no amplification was necessary to record the thermocouple output. The repeatability of the electromotive force calibration was about 2 percent for the linear output.

Model Pressure Gages

Pressure measurements on the flat plate were made with single-diaphragm variable-reluctance-type transducers. They were rated at 0.25 pound per square inch full scale with an excitation voltage of 5 volts at 20 kilocycles. The

response time of the transducers during the present investigation was well within the order of 1 millisecond at full scale as specified by the manufacturer.

The transducers were mounted in the support plate so that the orifice tube length was minimized to 3/8 inch to avoid unnecessary lag in the measurements. (See fig. 2.) Carrier amplification of the transducer output signal allowed pressure measurements as low as 0.005 psi to be made with reasonable accuracy. Calibration of each model pressure transducer was made over the pressure range anticipated for the test. The linear calibrations could be repeated within ±5 percent.

Table I shows two pressure orifice locations on each respective leading-edge piece (not shown in fig. 2). One pressure orifice was located at the same x- and y-coordinates on each leading-edge piece. The second orifice had the same y-coordinate but different x-coordinates for each leading edge.

DATA REDUCTION

Heat-Transfer Measurements

In order to obtain, reduce, and analyze the heat-transfer data, it was necessary to make the following assumptions, some of which are based on previous experience:

(1) The sensing skin was thin enough that the temperature of the undersurface was representative of the average temperature through the skin thickness. Calculations for the 0.002-inch-thick stainless-steel sensing surface at a stagnation point on a model indicated that the back-surface temperature was equal to that of the average front temperature, a thermal diffusivity of 5×10^{-5} ft^2/sec being considered.

(2) Heat losses from the periphery of the calorimeter sensing surface to the support structure were assumed to be negligible.

(3) Heat applied to the sensor entered the front surface only.

(4) Uniform heat distribution existed over the entire calorimeter surface.

(5) Constant thermal diffusivity existed throughout the sensing surface.

(6) The thermocouple wires sensed the back-surface temperature of the material.

(7) Heat loss along the length of the thermocouple wires was negligible. Calculations were made by assuming that the two wires attached to the underside of the sensing material were of equal diameter. These calculations indicated that for a constant q there was a heating-rate error for the two wires of about 3 percent at 20 milliseconds after heat was initially applied to the sensing surface.

(8) No heat sink existed at the junction of the thermocouple wires and sensing underside surface.

The factors which led to the validity of the preceding assumptions were as follows:

(1) The thin stainless-steel skin was precision rolled to a thickness of 0.002 inch ± 0.00005 inch.

(2) Handbook values of ρ and c were used, and the temperature rise of the disk material was kept to a few degrees above room temperature. Therefore, the density and specific heat were essentially constant.

(3) A linear thermoelement output curve was used.

(4) Since the diameter (0.25 inch) of the sensing disk was much larger than the thickness (0.002 inch), it was felt that the heat loss radially outward or to a sink at the disk periphery was negligible.

(5) The temperature gradient through the sensing surface was negligible and no loss due to wire length was experienced. It is believed that the heat-transfer slopes read from the records were accurate within 1 percent.

Therefore, since the thickness t_c (0.002 inch), specific heat c (0.12 Btu/lb-^{o}F), and density of the sensing material ($0.29\ lb/in^3$) were known, it may be seen from equation (4) that only the time derivative of the average surface temperature $dT/d\tau$ was necessary to obtain heat-transfer data. This derivative was actually determined by measuring the slope of each thermocouple output trace at discrete time intervals in terms of inches of deflection. The paper speed of each oscillograph record (ft/sec) together with the change in voltage per degree Fahrenheit for the chromel-alumel thermocouple wires $\left(\frac{44^{o}\ F}{millivolts}\right)$ and the calibration slope for each gage circuit $\left(\frac{millivolts}{ft}\right)$ were used to compute general heat-transfer-rate equation, as follows

$$\dot{q} = \rho c t_c \frac{dT}{d\tau} = \rho c t_c (44)(\text{paper speed})(\text{calibration slope})(\text{trace slope})$$

where $\dot{q}$ is measured in $\frac{Btu}{ft^2\text{-sec}}$.

Pressure Measurements

Prior to testing, a calibration of the pressure range anticipated for the test was made for the individual gages. Measurements were read from oscillograph records at 10-millisecond intervals with zero time selected as the first indication of a pressure rise.

Correction to Data

Until recently, it had been the practice of investigators in hotshot tunnels to define the flow by simultaneously measuring the test-section pitot pressure and the reservoir pressure, and from the known density of the initial charge of gas in the reservoir, to assume that the same density, uniformly distributed, existed in the reservoir after arc discharge. With these three parameters it was possible to calculate all the other characteristics of the flow with a suitable data-reduction program such as that used in reference 33. Recent work (refs. 34 and 35 and unpublished data from other facilities) has indicated that the assumption of uniform density in the reservoir may lead to serious error in flow definition. To define the flow more accurately, a series of tests was made for which simultaneous measurements of free-stream velocity, stagnation-point heat-transfer rate, and the previously mentioned pressures and density were obtained. These results yield correction factors that may be applied to test results for which the density was assumed to be uniformly distributed.

Several simultaneous measurements of the free-stream velocity and stagnation-point heat-transfer rate were made with the flat plate installed in the tunnel. All the data of the present investigation have been corrected by the factors which are presented in table II.

THEORY

Hypersonic Self-Induced Pressure Gradient on a Sharp Leading-Edge Flat Plate

Several investigations have shown that an asymptotic solution for large boundary-layer-induced pressures can be related to a physical plane pressure gradient $p \propto x^n$ if hypersonic and isentropic flow is assumed at the boundary-layer edge. (See refs. 36 to 39.)

Bertram and Feller (ref. 16) have presented an analysis which follows that of Li and Nagamatsu (ref. 36) for laminar boundary-layer flows in which an axial pressure gradient exists along the plate surface. Equations are presented in reference 16 which show that the induced pressure ratio, boundary-layer thickness, and local heat-transfer characteristics can be written as:

$$\frac{p_w}{p_\infty} = A\frac{M_\infty^3\sqrt{C_w}}{\sqrt{R_{\infty,x}}} \tag{5}$$

$$\frac{z_\delta}{x}\sqrt{\frac{R_{\infty,x}}{C_w}} = BM_\infty^2\left(\frac{\sqrt{R_{\infty,x}}}{M_\infty^3\sqrt{C_w}}\right)^{1/2} \tag{6}$$

$$\frac{N_{St,\infty}\sqrt{R_{\infty,x}}}{\sqrt{C_w}} = D\left(\frac{M_\infty^3\sqrt{C_w}}{\sqrt{R_{\infty,x}}}\right)^{1/2} \tag{7}$$

where A, B, and D are coefficients given by equations (21), (22), and (24) of reference 16. These coefficients are plotted in figure 9 of reference 16 as a function of wall-to-stagnation-temperature ratio for various values of γ. Equations (5) to (7) are applicable for a hypersonic self-induced pressure gradient on a flat plate for a strong interaction solution.

Bertram and Feller have also shown in reference 16 that from the analysis of Li and Nagamatsu (ref. 36) for hypersonic flow, where the Prandtl number is equal to unity and n (exponent of $p \propto x^n$) may have positive or negative values, the heat-transfer coefficients may be expressed as the ratio

$$\frac{h}{\bar{h}} = K_3\sqrt{\frac{p_w}{p_\infty}} \tag{8}$$

where $\bar{h}$ represents the case in which $dp/dx = 0$. The coefficient K_3 is defined by equation (9) of reference 16 and accounts for the effect of the pressure gradient. The amount that K_3 deviates from unity is a measure of the importance of this gradient apart from the effect of changes in local conditions. It was found earlier that K_3 was relatively insensitive to changes in wall temperature and γ for the insulated-wall case. The square root of the pressure ratio accounts for differences between local and undisturbed free-stream conditions. The following sketches are typical of the model used for the numerical computations of the preceding theory for boundary-layer displacement and blast-wave analysis.

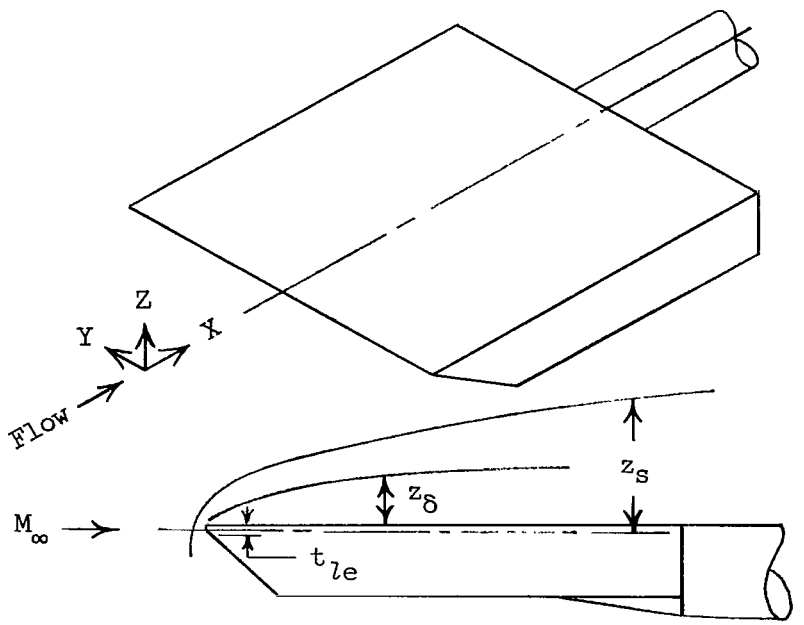

Sketch (A).- Flat plate at $\alpha = 0^o$.

Pressure Distribution for Blunt Leading-Edge Flat Plate at $\alpha = 0^\circ$

Inviscid effect.- The inviscid effect of blunt leading edges usually dominates the induced pressure and heat transfer for high Mach number low-density flow for several nose diameters downstream of the leading edge. This effect results from an entropy jump at the leading edge near the plate surface. In particular, Bertram and Blackstock (ref. 21) have shown that the addition of the pressure increment obtained from tangent-wedge theory to the increment due to blunting the leading edge on a flat plate, gave results which were in good agreement with the characteristic theory. (See ref. 6.) Therefore, for the case where $p_w/p_\infty \geq 1.2$, the blunt-leading-edge inviscid effects can be expressed in the form

$$\frac{p_w}{p_\infty} = 0.187\epsilon\left[\sqrt{\gamma}(\gamma - 1)\frac{M_\infty^3 C_D}{x/t_{le}}\right]^{2/3} + 0.74 \tag{9}$$

where

$$\epsilon \approx 1 - \left[0.0048(\gamma - 1)^2\right]$$

and represents a small correction term to the function of γ in equation (9).

Small viscous effects.- If the blunt-leading-edge induced pressures are assumed to be much larger than the viscous induced-pressure increment and somewhat larger than the free-stream pressure, the tangent-wedge portion of the solution can be obtained, as in reference 21, through proper substitution of the equation representing the slope of the boundary-layer edge in hypersonic similarity form into the first-order equation representing hypersonic small-perturbation theory. The completed expression for this solution is

$$\frac{\Delta p_{viscous}}{p_\infty} = \frac{5}{6}\frac{\gamma G \bar{\chi}_\infty}{\sqrt{p_w/p_\infty}} \tag{10}$$

where for the Prandtl number of 0.725 of this investigation

$$G = 1.648\frac{\gamma - 1}{2}\left(\frac{T_w}{T_r} + 0.352\right)$$

If equation (9) is added to equation (10), an account of the inviscid plus weak viscous interaction effects can be evaluated empirically with some degree of accuracy.

Strong viscous effects.- If the viscous-induced increment in pressure is too large to be ignored and contributes sufficiently to the induced effect on the boundary-layer growth, the effect must be accounted for. Bertram and

Blackstock (ref. 21) have developed an equation which when used with the inviscid case should predict with some degree of accuracy the effects of inviscid and strong viscous interaction. By the substitution of the strong interaction equation in terms of boundary-layer slope (eq. (15) of ref. 21) into the expression for the hypersonic similarity deflection angle (based on the edge of the boundary layer), the equation for strong viscous effects becomes

$$\frac{\Delta p_{viscous}}{p_\infty} = \frac{1}{2}\left\{\sqrt{\left(\frac{p_w}{p_\infty}\right)^2 + \frac{\gamma(\gamma+1)}{2}\left[(1-n)K_4\right]^2\left(G\bar{X}_\infty\right)^2} - \frac{p_w}{p_\infty}\right\} \tag{11}$$

Therefore, to account for both the inviscid and strong viscous effects, equation (11) may be added to equation (9). In equation (11), n is the exponent in the power equation for the surface pressure variation with x, $p_w \propto x^n$. In the equation of the hypersonic-similarity theory K_4 is a coefficient varying with laminar boundary-layer growth, and is expressed as a function of pressure gradient and wall-to-stagnation temperature ratio at various values of γ. (See fig. 1 of ref. 21.)

Shock-Wave Shapes

Many approaches to the blast-wave concept have been made (refs. 1 to 6). For inviscid hypersonic flow over a simple slender two-dimensional body, Lukasiewicz (ref. 1) has shown that approximate solutions of blast analogy can be derived for plane or axisymmetric flow. Reference 1 has shown that for $\gamma = 1.4$ and plane flow at zero angle of attack, the following expression exists for shock-wave shapes to the first approximation

$$\frac{\frac{z_s}{t_{le}}}{M_\infty^2 C_D} = 0.774\frac{\left(\frac{x}{t_{le}}\right)^{2/3}}{M_\infty^2 C_D^{2/3}} \tag{12}$$

and to the second approximation

$$\frac{\frac{z_s}{t_{le}}}{M_\infty^2 C_D} = \frac{0.774}{\frac{M_\infty^2 C_D^{2/3}}{\left(\frac{x}{t_{le}}\right)^{2/3} - 1.09}} \tag{13}$$

Correlation of Experimental Data

A theoretical correlation value for the undisturbed flat-plate Stanton number may be obtained by various means where $dp/dx = 0$. (See refs. 16, 25, and 38.) In this presentation, the T' method and modified Reynolds number analogy were applied to the Blasius skin-friction value to obtain the correlation parameter for the Stanton number (ref. 40).

$$N_{St,\infty} = 0.332 N_{Pr,\infty}^{-2/3} R_{\infty,x}^{-1/2} (C')^{1/2} \tag{14}$$

where $C' = \dfrac{\mu_\infty' T_\infty}{\mu_\infty T'}$ and where $N_{Pr,\infty}^{-2/3}$ is the Reynolds number analogy factor evaluated at T'. (See ref. 31.)

To evaluate the viscosity-temperature ratio, Monaghan expresses the T' equation in reference 31 as

$$\frac{T'_\infty}{T_\infty} = \frac{T_w}{T_\infty} + 0.468 N_{Pr,\infty}^{1/3} \left(\frac{T_r}{T_\infty} - \frac{T_w}{T_\infty} \right) - 0.273 N_{Pr,\infty} \left(\frac{\gamma - 1}{2} \right) M_\infty^2 \tag{15}$$

Bertram and Feller (ref. 16) have further shown that for very high Mach numbers ($N_{Pr,\infty}$ = Constant), equation (15) becomes

$$\frac{T'}{T_t} = \frac{T_w}{T_t} \left(1 - 0.468 N_{Pr,\infty}^{1/3} \right) + 0.468 N_{Pr,\infty}^{5/6} - 0.273 N_{Pr,\infty} \tag{16}$$

From equation (16), the T' temperature becomes constant for a given ratio of wall temperature to stagnation temperature. In this presentation, a value of 0.72 was used for the Prandtl number and equation (16) becomes

$$\frac{T'}{T_t} = 0.160 + 0.580 \frac{T_w}{T_t} \tag{17}$$

If the assumption is made that equation (14) is valid when local conditions are utilized along with constant wall pressure, the blunt flat plates can be simply evaluated by assuming that the flow over the plate has passed through a normal shock and the flow at the boundary-layer edge is at constant pressure (the sharp leading-edge plate is considered as having a degree of bluntness). To account for the case where $dp/dx \neq 0$, the heat-transfer-coefficient ratio which has been given in equation (8) as

$$\frac{h}{\bar{h}} = K_3 \sqrt{\frac{p_w}{p_\infty}}$$

is used for hypersonic flow with a Prandtl number of 1 (Li and Nagamatsu; ref. 36), for positive or negative values of n, and $\bar{h}$ representing the value for which the pressure gradient is zero (dp/dx = 0). To evaluate the sharp or blunt leading-edge case, equation (8) was multiplied by equation (14) to obtain

$$N_{St,\infty}\sqrt{R_{\infty,x}} = \frac{0.332}{N_{Pr,\infty}^{2/3}} K_3 \sqrt{\frac{p_w}{p_\infty}} \tag{18}$$

The measured pressure distributions in this expression can also be used to give an independent check of the measured and calculated heat-transfer distributions. Equation (18) may be used to determine an error existing in the heat-transfer parameter. In each case, the experimental pressure data were fitted according to the power law, $p \propto x^n$.

RESULTS AND DISCUSSION

General

Figure 3 shows the typical variation and reproducibility of the measured local heat-transfer and pressure distribution for two successive runs on the sharp flat plate at angles of attack and yaw of 0°. In general, the accuracy and repeatability of the data were satisfactory.

At least two tunnel tests were made for each of the leading-edge bluntnesses. The magnitude and distribution of the heat transfer indicate that the boundary layer was laminar. Because of somewhat higher heat-transfer rates at the most downstream stations it is suspected that in some instances there may have been some type of trailing-edge influence on the last few gage locations. The discussion regarding spanwise variations in pressure and heat transfer is very brief since the small model volume allowed only a limited number of gages to be installed. Therefore, the two streamwise rows (see fig. 2) are given emphasis.

A nominal set of flow conditions for theory was used for the test conditions noted on the figures since the conditions tested were nearly the same. Thus, there exists in each case only one theoretical curve rather than two.

Spark schlieren photographs were taken during each test. In each case, a no-flow picture was taken to determine flaws in the test-section schlieren windows. The windows produced negligible image distortion. In some cases misalinement of the schlieren system was suspected, so that the true shock standoff distance could not be determined. Typical schlieren photographs are shown in figure 4. Flaws in the window are evident in the photographs. The outer edge of the boundary layer can be distinguished in figure 4(a) for the sharp leading edge (t = 0.0003 inch). As the leading-edge bluntness is increased, the density decreases near the plate surface. With sufficient blunting, the boundary layer

becomes undetectable as shown in figure 4(d). The apparent reduction in schlieren sensitivity contributed to the decrease in the ability to detect the boundary layer in figure 4.

Sharp flat plate.- Figure 5 shows the comparison between theory and experiment in terms of the pressure ratio (at top of figure) and the heat-transfer-correlation parameter $N_{St,\infty}\sqrt{R_{\infty,x}}$ for two runs for the sharp flat plate at zero angle of attack. The variations of the pressure ratio and the heat-transfer-correlation parameter with Reynolds number based on the distance from the leading edge along the plate surface are plotted in figure 5. The open symbols represent a spanwise location of $y = \pm 0.75$ inch from the center line and the solid symbols are for ± 0.25 inch from the center line. (See fig. 2 and table I.) Pressure data for gages 16 and 17 (for $x = 3.50$ inches and $y = 1.25$ inches and $y = 1.75$ inches) were not plotted and neither were the data for heat-transfer gages 16, 17, and 18 (for $x = 3.50$ inches and $y = 1.25$, $y = 1.75$, and $y = 2.25$ inches). The data, in general, showed a spanwise decrease at these stations. There seems to be no spanwise effect within the range represented by the open symbols.

The induced pressure theory (eq. (5)) was applied and was found to agree with the data over most of the sharp plate, although it was somewhat higher near the leading edge. The discrepancy between theoretical and experimental results near the leading edge is believed to be due to a transition between continuum and free-molecular flow since the Knudsen number for the present experimental investigation on the sharp leading-edge plate was calculated to be about 2.5. Some other tests were made on the sharp plate in addition to those presented herein to give some insight into the extent the transition flow existed on the sharp leading-edge plate. With an increase in Knudsen number the reduction in pressure and heat transfer near the leading edge of the plate was experienced over a longer length of the plate and an increase in the slip or transition region was indicated. These preliminary results are similar to those of references 22 to 24 and 26. A slope of $n = -0.500$ was used for the strong-interaction theory. A value for K_3 in equation (8) was obtained for $\gamma = 7/5$ from figure 6 of reference 16.

The strong-interaction theory for the pressure distribution (which is in good agreement with the pressure data) was used in equation (18) to calculate $N_{St,\infty}\sqrt{R_{\infty,x}}$ and this strong-interaction theory is compared with the experimental data in the lower plot of figure 5. Both the experimental data and the strong-interaction theory have a somewhat higher trend than the hypersonic similarity theory (eq. (7)), which is also shown in figure 5. This result is not surprising since equation (18) is a more general form of equation (7). (See ref. 16.) The results from sharp leading-edge theory for the Stanton number correlating parameter, given by equation (14) $\left(\text{zero-pressure-gradient theory, } p_w = p_\infty, \frac{dp}{dx} = 0\right)$, were also compared with the experimental data and illustrate the effect of pressure gradient on hypersonic heat transfer.

Blunt flat plate.- Equation (18) was used to correlate the experimental data plotted in figures 6, 7, and 8. Again, the pressure ratio, plotted at the top of each figure, was fitted by the power law and the values of n were used to obtain K_3.

Estimations of the experimental pressure distribution for each leading-edge bluntness were obtained by individually adding the results from equations (10) and (11) to those of equation (9). For each bluntness, the weak viscous effects (eqs. (9) and (10)) fell below the experimental data near the leading edge, but approached good agreement at the most downstream stations for increased leading-edge bluntness. In all cases, the strong viscous effects (eq. (9) and eq. (11)) agreed well with the experimental pressure distribution, except near the leading edge where the theoretical result is lower than experimental results predicted. Experimental pressure data in reference 26 were obtained for test conditions similar to those of the present investigation for Mach numbers of 18.3 and 18.7 and $110 < R_t < 630$; however, the ratio of wall temperature to stagnation temperature was somewhat smaller and the Knudsen number larger in reference 26. The data of reference 26 showed good agreement with the inviscid theory and were approximately 50 percent below the theory for inviscid plus viscous interaction in contrast to the present results. Although the ratio of wall enthalpy to stagnation enthalpy of reference 26 was lower than that in the present investigation, it is felt that the primary cause for the differences in the two sets of data stems from Burke's Knudsen number being several times larger than in the present results.

Only the inviscid plus strong viscous effects (eq. (9) and eq. (11)) were correlated in terms of $N_{St,\infty}\sqrt{R_{\infty,x}}$ and plotted in the lower half of figures 6, 7, and 8. The slopes n were determined and were used to evaluate K_3. The simple addition of equation (9) and equation (11) indicates good agreement with the correlated experimental pressure results, but the result was considerably lower than the experimental heat-transfer data.

At the present, there are several theoretical approaches to cover the real case where both viscous and inviscid effects occur. One approach is to add linearly the two effects. (See refs. 21, and 41 to 43.) This linear-addition approach should be considered nearly valid only if one effect is small compared with the other and even then it should not be considered completely valid.

Sharp Flat-Plate Boundary-Layer Thickness

A check of hypersonic similarity based on measured boundary-layer thickness is difficult because the definition of boundary-layer thickness is arbitrary. However, it was felt that some insight into the sharp-leading-edge flat plate could be gained from the present investigation by measuring the apparent boundary-layer thickness from schlieren photographs.

Figure 9 shows the boundary-layer thickness plotted against the distance from the leading edge. The boundary-layer measurements were made from the plate surface to the outer edge of the boundary layer. (See sketch (A).) The dark line in figure 4(a) denotes the region of large density gradient normal to the surface and corresponds approximately with the surface of the thermal boundary layer. The boundary layer shown in figure 4(a) is not sharply defined, and, therefore, the measurement is only an approximation. It is felt, however, that the data are to a large extent representative of the boundary-layer thickness. The result of the hypersonic boundary-layer theory expressed by equation 6 shows fair agreement with the measured thickness. It can be seen that for the sharp plate the boundary layer is merged with the shock layer near the leading edge (given previously in refs. 22 and 23). Boundary-layer thickness in the present study is about 0.65 inch at a distance of 7 inches from the leading edge.

The concept of including local pressure distribution through the use of standard hypersonic approximations can be shown by simply multiplying the boundary-layer-thickness equation (eq. (6)) by the square root of the local pressure ratio. (See fig. 10.) The equation becomes

$$\frac{z_\delta}{x}\sqrt{\frac{R_{\infty,x}}{C_w}}\sqrt{\frac{p_w}{p_\infty}} = BM_\infty^2\left(\frac{\sqrt{R_{\infty,x}}}{M_\infty^3\sqrt{C_w}}\right)^{1/2}\sqrt{\frac{p_w}{p_\infty}} \tag{19}$$

The bottom part of figure 10 shows the boundary-layer thickness in terms of the correlating parameter given by the zero-pressure-gradient theory (eq. (6)) plotted against Reynolds number based on plate-surface displacement. The correlating parameter decreases with decreasing Reynolds number. At the top of figure 10, a modification of the boundary-layer-thickness parameter has been made as suggested by reference 16 to include the variation of local pressure conditions. Equation (19) was employed and also shows good agreement when the results were plotted against Reynolds number. Figure 10 indicates that the experimental results are essentially independent of the distance x, as was predicted by theory.

Shock Shapes From Schlieren Photographs

Figure 4 consists of representative photographs of the different leading-edge bluntnesses tested at nearly constant Reynolds and Mach numbers. The shock shape is essentially determined by the mutual interaction of the shock wave and boundary layer for the sharp plate near the leading edge (fig. 4(a)). This merged interaction occurs for $R_t = 11.5$ at the conditions tested, as has been noted previously by others for similar small R_t values. The schlieren photograph (fig. 4(a)) for the sharp plate is believed to be somewhat similar to those obtained by Nagamatsu (refs. 22 to 24) for free-molecule flow

conditions. Nagamatsu indicates that for large Knudsen numbers, very small R_t values, and high flow velocities, the flow at the leading edge is nearly free molecular. This free-molecular flow is followed by a rarefied flow, and finally attains at the end of the slip distance the continuum flow regime with a velocity at the wall equal to zero. These conditions are illustrated in sketch (B).

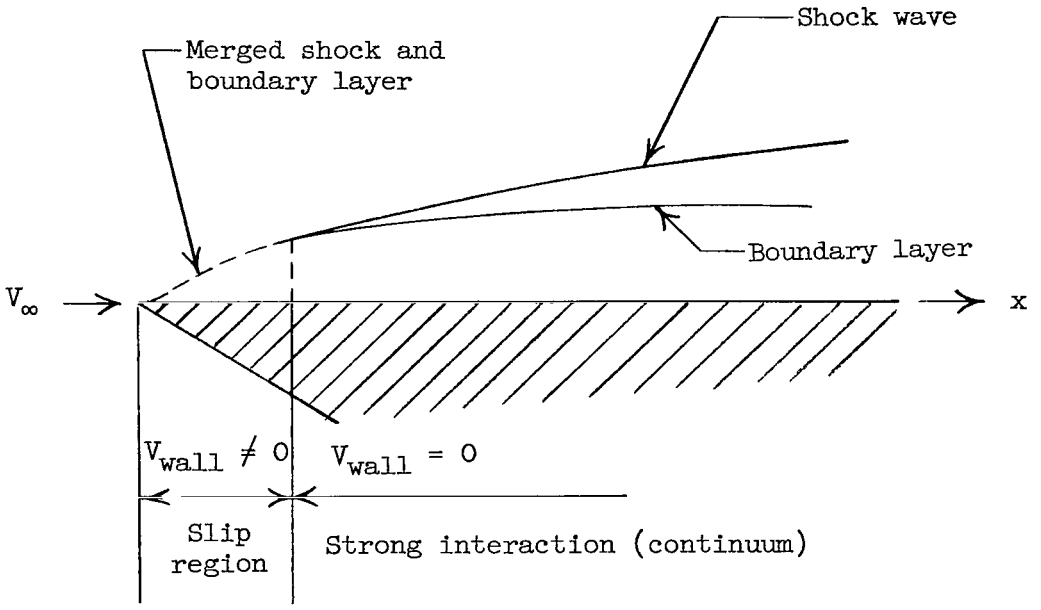

Sketch (B).- Flow conditions for sharp plate.

It was found in the present investigation on the sharp plate that the merged layer slope increased from the leading edge to some maximum value near the end of the slip region. The shock wave and boundary layer are both merged and their formation was delayed in this region.

The shock-wave coordinates for the various bluntnesses measured from the photographs (see sketch (A)) are presented in figure 11. Qualitatively, the shock shapes are similar to those observed by others for hypersonic-flow and adiabatic-wall conditions. (See refs. 25 and 43.) The shock wave for the sharp plate appears to be attached. Only slight detachment and standoff occurs for the blunt leading-edge plates.

First-approximation blast-wave theory does not agree with the experimental shock shapes for any of the leading-edge configurations. (See fig. (12).) The second approximation, in general, provides a much closer prediction of the experimental shapes and an even closer prediction was obtained from the theory of Cheng and Pallone (ref. 4). As expected, the agreement between theoretical blast-wave shapes and the experimental shock shapes improves with an increase in

leading-edge bluntness. It is believed that the outward displacement of the shock wave downstream is due to the large boundary-layer displacement effects. Somewhat similar results have been noticed previously by other investigators (refs. 25 and 26).

CONCLUSIONS

An investigation of high Mach number low-density flow over a flat plate with variation in leading-edge bluntness has been made. The investigation included effects of leading-edge bluntness and viscous interaction at zero angle of attack. Pressure and heat-transfer data as well as schlieren photographs were obtained in the Langley hotshot tunnel. The nominal test conditions were a Mach number of approximately 20, a stagnation temperature of 4000° R, and a Reynolds number per foot of approximately 0.46×10^6. Correlations and comparisons of the experimental results with hypersonic flow theory have led to the following conclusions:

1. Available theoretical methods are adequate for prediction of the pressure distributions on a blunt flat plate; however, the measured heat-transfer distributions are always somewhat higher than the theory.

2. The experimental pressure distribution on the sharp leading-edge plate can be predicted by the strong interaction theory where continuum flow exists.

3. The hypersonic boundary-layer theory was found to account satisfactorily for the variations in boundary-layer thickness due to the variations in pressure distributions on the sharp plate.

4. The theory of Cheng and Pallone predicted the shock shapes better than did the first- or second-order blast-wave approximation theory.

Langley Research Center,
National Aeronautics and Space Administration,
Langley Station, Hampton, Va., May 19, 1965.

REFERENCES

1. Lukasiewicz, J.: Hypersonic Flow-Blast Analogy. AEDC-TR-61-4, U.S. Air Force, June 1961.

2. Lin, Shao-Chi: Cylindrical Shock Waves Produced by Instantaneous Energy Release. J. Appl. Phys., vol. 25, no. 1, Jan. 1954, pp. 54-58.

3. Lees, Lester; and Kubota, Toshi: Inviscid Hypersonic Flow Over Blunt-Nosed Slender Bodies. J. Aeron. Sci., vol. 24, no. 3, Mar. 1957, pp. 195-202.

4. Cheng, H. K.; and Pallone, A. J.: Inviscid Leading-Edge Effect in Hypersonic Flow. J. Aeron. Sci. (Readers' Forum), vol. 23, no. 7, July 1956, pp. 700-702.

5. Chernyi, G. G.: Hypersonic Flow Past an Airfoil With a Slightly Blunted Leading Edge. C-112, Morris D. Friedman, Inc. (Needham Heights 94, Mass.). (From Doklady Akademii Nauk U.S.S.R., vol. 114, no. 4, 1957, pp. 721-724.)

6. Baradell, Donald L.; and Bertram, Mitchel H.: The Blunt Plate in Hypersonic Flow. NASA TN D-408, 1960.

7. Hayes, Wallace D.; and Probstein, Ronald F.: Hypersonic Flow Theory. Academic Press, Inc. (New York), 1959.

8. Moore, F. K.; and Cheng, H. K.: The Hypersonic Aerodynamics of Slender and Lifting Configurations. Paper No. 59-125, Inst. Aeron. Sci., June 1959.

9. Bertram, Mitchel H.: An Approximate Method for Determining the Displacement Effects and Viscous Drag of Laminar Boundary Layers in Two-Dimensional Hypersonic Flow. NACA TN 2773, 1952.

10. Lees, Lester; and Probstein, Ronald F.: Hypersonic Viscous Flow Over a Flat Plate. Rept. No. 195 (Contract AF 33(038)-250), Aeron. Eng. Lab., Princeton Univ., Apr. 20, 1952.

11. Shen, S. F.: On the Boundary-Layer Equations in Hypersonic Flow. J. Aeron. Sci. (Readers' Forum), vol. 19, no. 7, July 1952, pp. 500-501.

12. Li, Ting-Yi; and Nagamatsu, H. T.: Shock-Wave Effects on the Laminar Skin Friction of an Insulated Flat Plate at Hypersonic Speeds. J. Aeron. Sci., vol. 20, no. 5, May 1953, pp. 345-355.

13. Lees, Lester: On the Boundary-Layer Equations in Hypersonic Flow and Their Approximate Solutions. J. Aeron. Sci., vol. 20, no. 2, Feb. 1953, pp. 143-145.

14. Pai, Shih-I.: A Note on Hypersonic Viscous Flow Over a Flat Plate. J. Aeron. Sci. (Readers' Forum), vol. 20, no. 7, July 1953, pp. 502-504.

15. Lees, L.: Hypersonic Viscous Flow Over an Inclined Wedge. J. Aeron. Sci. (Readers' Forum), vol. 20, no. 11, Nov. 1953, pp. 794-796.

16. Bertram, Mitchel H.; and Feller, William V.: A Simple Method for Determining Heat Transfer, Skin Friction, and Boundary-Layer Thickness for Hypersonic Laminar Boundary-Layer Flows in a Pressure Gradient. NASA MEMO 5-24-59L, 1959.

17. Oguchi, Hakuro: First-Order Approach to a Strong Interaction Problem in Hypersonic Flow Over an Insulated Flat Plate. Rept. No. 330, Aeron. Res. Inst., Univ. Tokyo, June 1958.

18. Lees, Lester: Recent Developments in Hypersonic Flow. Jet Propulsion, vol. 27, no. 11, Nov. 1957, pp. 1162-1178.

19. Lees, Lester: Influence of the Leading-Edge Shock Wave on the Laminar Boundary Layer at Hypersonic Speeds. J. Aeron. Sci., vol. 23, no. 6, June 1956, pp. 594-600, 612.

20. Pan, L. J.; and Kuo, Y. H.: Compressible Viscous Flow Past a Wedge Moving at Hypersonic Speeds. J. Math. Phys., vol. XXXV, no. 2, July 1956, pp. 179-193.

21. Bertram, Mitchel H.; and Blackstock, Thomas A.: Some Simple Solutions to the Problem of Predicting Boundary-Layer Self-Induced Pressures. NASA TN D-798, 1961.

22. Nagamatsu, H. T.; Weil, J. A.; and Sheer, R. E., Jr.: Leading Edge Bluntness and Slip Flow Effects in High Temperature Hypervelocity Flow Over a Flat Plate. Presented at AGARD Specialists' Meeting "High Temperature Aspects of Hypersonic Flow" (Rhode-Saint-Genese, Belgium), Apr. 3-6, 1962. (Available from ASTIA as AD No. 283 501.)

23. Nagamatsu, H. T.; Weil, J. A.; and Sheer, R. E., Jr.: Heat Transfer to Flat Plate in High Temperature Rarefied Ultrahigh Mach Number Flow. ARS J., vol. 32, no. 4, Apr. 1962, pp. 533-541.

24. Nagamatsu, H. T.; Sheer, R. E., Jr.; Weil, J. A.: Rarefied High-Temperature, Ultrahigh Mach Number Slip Flow Over a Sharp Flat Plate. Rept. No. 63-RL-(3285C), Gen. Elec. Res. Lab., Apr. 1963. (Available from ASTIA as AD No. 432130.)

25. Cheng, H. K.; Hall, J. Gorden; Golian, T. C.; and Hertzburg, A.: Boundary-Layer Displacement and Leading-Edge Bluntness Effects in High-Temperature Hypersonic Flow. J. Aerospace Sci., vol. 28, no. 5, May 1961, pp. 353-381, 410.

26. Burke, A. F.; Smith, W. C.; Dowling, E. D.; and Carlson, D. R.: Lifting Surfaces in Rarefield Hypersonic Airflow. Part I: The Effects of Bluntness and Angle of Attack on the Flow Over a Flat Plate. Rept. No. AA-1596-Y-1(ASD-TDR 62-797, Pt. I), Cornell Aeron. Lab., Inc., Dec. 1962.

27. Vas, I. E.; and Bogdonoff, S. M.: Mach and Reynolds Number Effects on the Flows Over Blunt Flat Plates at Hypersonic Speeds. Rept. 529 (ARL Tech. Note 60-164), Dept. Aeron. Eng., Princeton Univ., Nov. 1960.

28. Hammitt, A. G.; Vas, I. E.; and Bogdonoff, S. M.: Leading Edge Effects on the Flow Over a Flat Plate at Hypersonic Speeds. Rept. No. 326 (Contract AF 33(616)-2547), Princeton Univ., Dept. Aeron. Eng., Sept. 1955.

29. Bertram, M. H.: Viscous and Leading-Edge Thickness Effects on the Pressures on the Surface of a Flat Plate in Hypersonic Flow. J. Aeron. Sci. (Readers' Forum), vol. 21, no. 6, June 1954, pp. 430-431.

30. Henderson, Arthur, Jr.; and Johnston, Patrick J.: Fluid-Dynamic Properties of Some Simple Sharp- and Blunt-Nosed Shapes at Mach Numbers from 16 to 24 in Helium Flow. NASA MEMO 5-8-59L, 1959.

31. Monaghan, R. J.: An Approximate Solution of the Compressible Laminar Boundary Layer on a Flat Plate. R. & M. No. 2760, British A.R.C., 1953.

32. Smith, Fred M.; Harrison, Edwin F.; and Lawing, Pierce L.: Description and Initial Calibration of the Langley Hotshot Tunnel With Some Real-Gas Charts for Nitrogen. NASA TN D-2023, 1963.

33. Grabau, Martin; Humphrey, Richard L.; and Little, Wanda J.: Determination of Test-Section, After-Shock, and Stagnation Conditions in Hotshot Tunnels Using Real Nitrogen at Temperatures From 3000 to 4000°K. AEDC-TN-61-82, U.S. Air Force, July 1961.

34. Ball, Henry W.: Calibration of the 100-Inch Hypervelocity Tunnel (F). AEDC-TDR-63-46, U.S. Air Force, Mar. 1963.

35. Karamcheti, Krishnamurty; Vali, Walter; Kyser, James B.; and Rasmussen, Maurice L.: Measurements of Pressure and Speed of Flow in a Spark-Heated Hypersonic Wind Tunnel. AEDC-TDR-62-218 (ASTIA Doc. No. 288668), Arnold Eng. Dev. Center, Nov. 1962.

36. Li, T. Y.; and Nagamatsu, H. T.: Hypersonic Viscous Flow on a Noninsulated Flat Plate. GALCIT Mem. No. 25 (Contract No. DA-04-495-Ord-19), Apr. 1, 1955.

37. Falkner, V. M.; and Skan, Sylvia W.: Some Approximate Solutions of the Boundary Layer Equations. R. & M. No. 1314, British A.R.C., 1930.

38. Hartree, D. R.: On an Equation Occurring in Falkner and Skan's Approximate Treatment of the Equations of the Boundary Layer. Proc. Cambridge Phil. Soc., vol. XXXIII, pt. 2, Apr. 1937, pp. 223-239.

39. Smith, A. M. O.: Improved Solutions of the Falkner and Skan Boundary Layer Equation. Rept. No. ES 16009 (Contract No. Noa(S)9027), Douglas Aircraft Co., Inc., Mar. 31, 1952.

40. Van Driest, E. R.: Investigation of Laminar Boundary Layer in Compressible Fluids Using the Crocco Method. NACA TN 2597, 1952.

41. Creager, Marcus O.: Effects of Leading-Edge Blunting on the Local Heat Transfer and Pressure Distributions Over Flat Plates in Supersonic Flow. NACA TN 4142, 1957.

42. Bertram, Mitchel H.; and Henderson, Arthur, Jr.: Effects of Boundary-Layer Displacement and Leading-Edge Bluntness on Pressure Distribution, Skin Friction, and Heat Transfer of Bodies at Hypersonic Speeds. NACA TN 4301, 1958.

43. Hammitt, A. G.; and Bogdonoff, S. M.: Hypersonic Studies of the Leading Edge Effect on the Flow Over a Flat Plate. Jet Propulsion, vol. 26, no. 4, Apr. 1956, pp. 241-246, 250.

TABLE I

COORDINATES AT GAGE LOCATIONS

[x referenced from leading-edge base line;
y referenced from center line]

Gage	Thermocouple		Pressure orifice	
	x, in.	y, in.	x, in.	y, in.
1	0.25	1.25	0.25	-0.25
2	.25	.25	.25	-1.25
3	.50	.75	.90	-.75
4	.75	.25	.75	-.25
5	1.00	.75	1.0	-.75
6	1.25	.25	1.25	-.25
7	1.50	.75	1.90	-.75
8	1.75	.25	1.75	-.25
9	2.00	.75	2.00	-.75
10	2.25	.25	2.25	-.25
11	2.50	.75	2.50	-.75
12	2.75	.25	2.75	-.25
13	3.00	.75	3.00	-.75
14	3.25	.25	3.25	-.25
15	3.50	.75	3.50	-.75
16	3.50	1.25	3.50	-1.25
17	3.50	1.75	3.50	-1.75
18	3.50	2.25	3.75	-.25
19	3.75	2.5	4.25	-.25
20	4.25	2.5	4.75	-.25
21	4.75	2.5		

Leading-edge configuration	Pressure gage 1A (*)		Pressure gage 1B (*)	
	x, in.	y, in.	x, in.	y, in.
1	0.197	0.12	0.0689	0.50
2	.170	.12	.068	.50
3	.130	.12	.066	.50
4	.080	.12	.066	.50

*Not shown in figure 2.

TABLE II.- CORRECTION FACTORS AS A FUNCTION OF TIME

[Subscript vel denotes velocity corrected data; subscript cal denotes uncorrected data]

Time, msec	$\frac{(\rho_{arc})_{vel}}{(\rho_{arc})_{cal}}$	$\frac{(T_{arc})_{vel}}{(T_{arc})_{cal}}$	$\frac{(p_\infty)_{vel}}{(p_\infty)_{cal}}$	$\frac{(\rho_\infty)_{vel}}{(\rho_\infty)_{cal}}$	$\frac{(T_\infty)_{vel}}{(T_\infty)_{cal}}$	$\frac{(V_\infty)_{vel}}{(V_\infty)_{cal}}$	$\frac{(M_\infty)_{vel}}{(M_\infty)_{cal}}$	$\frac{(R_\infty)_{vel}}{(R_\infty)_{cal}}$	$\frac{(T_t)_{vel}}{(T_t)_{cal}}$
0	1.45	0.66							
10	1.46	.75	0.95	1.39	0.69	0.85	1.03	1.88	0.74
20	1.30	.77	.97	1.36	.72	.86	1.02	1.78	.76
30	1.28	.78	.94	1.33	.71	.87	1.03	1.78	.78
40	1.27	.79	.95	1.30	.73	.88	1.03	1.70	.79
50	1.25	.81	.96	1.26	.76	.90	1.02	1.59	.81
60	1.22	.83	.97	1.23	.79	.91	1.02	1.51	.83
70	1.19	.86	.98	1.19	.82	.92	1.01	1.40	.86
80	1.16	.88	.98	1.16	.85	.93	1.01	1.33	.88
90	1.13	.90	.99	1.13	.87	.94	1.00	1.28	.89
100	1.12	.93	1.0	1.10	.91	.95	1.00	1.19	.92

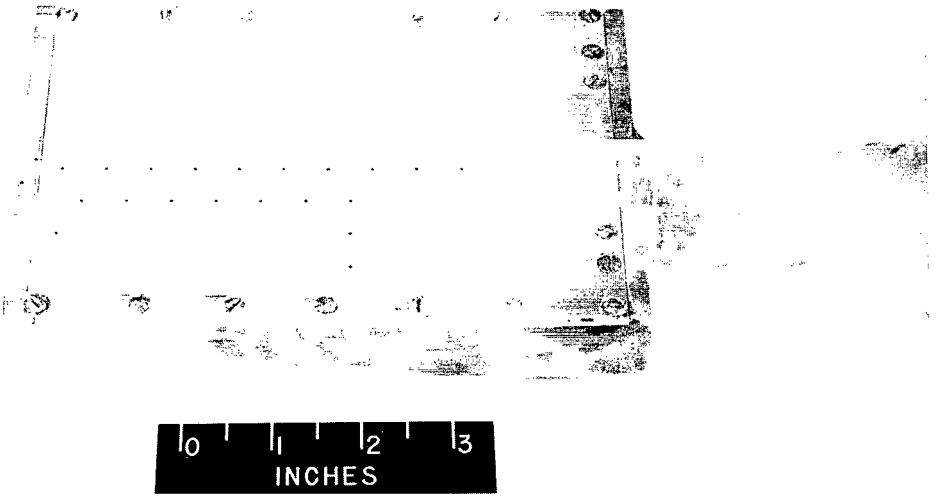

(a) Model. L-64-6875

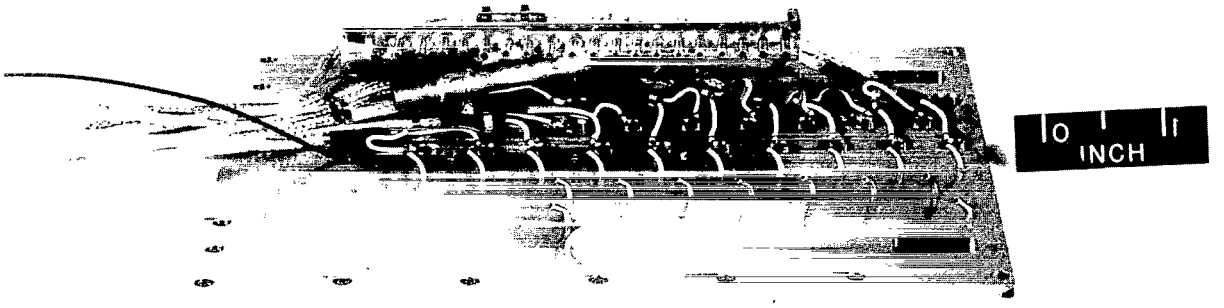

(b) Underside of instrumented surface. L-63-8643

Figure 1.- Photograph of model and instrumented surface.

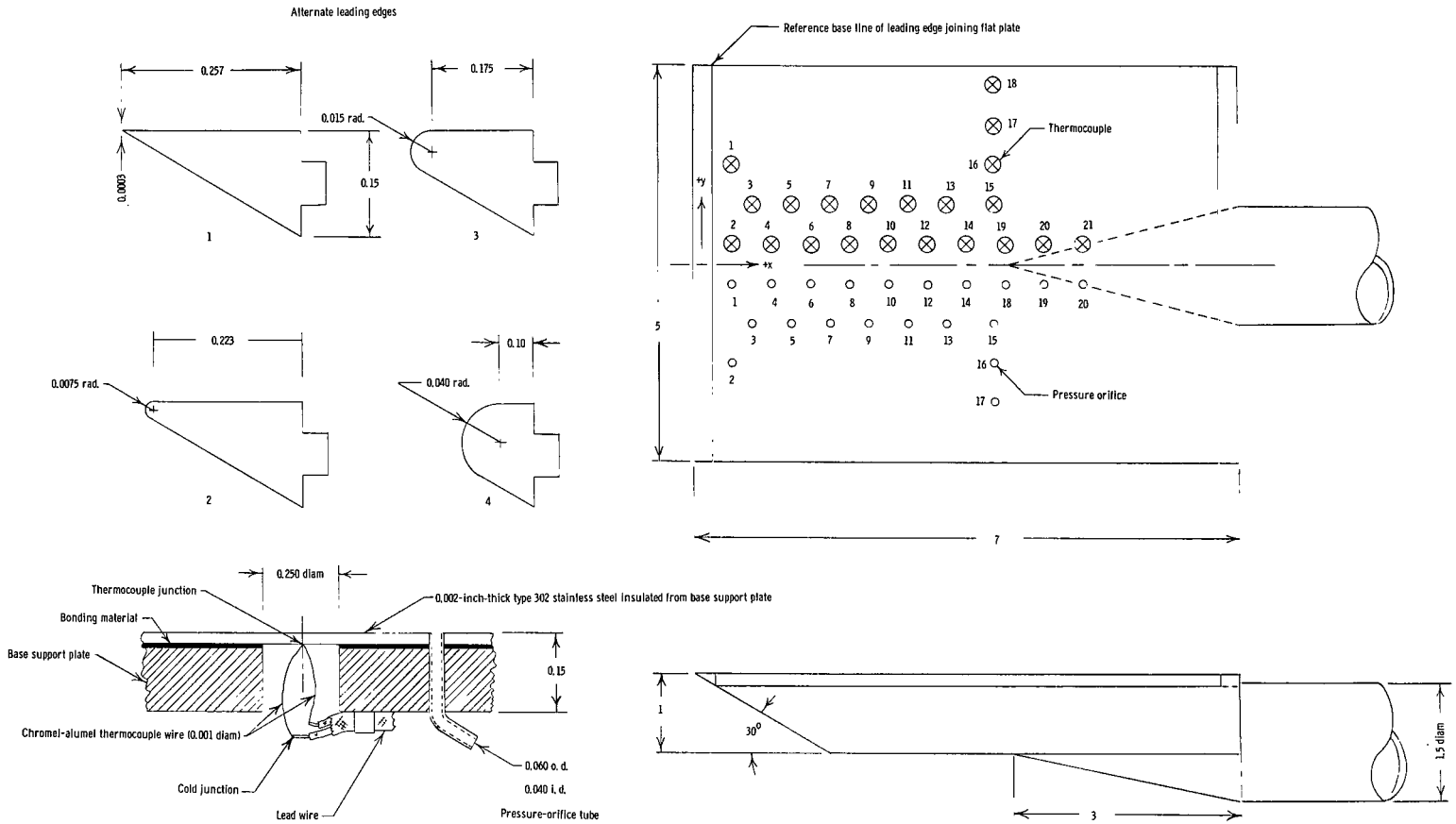

Figure 2.- Flat-plate model. All dimensions are in inches unless otherwise noted.

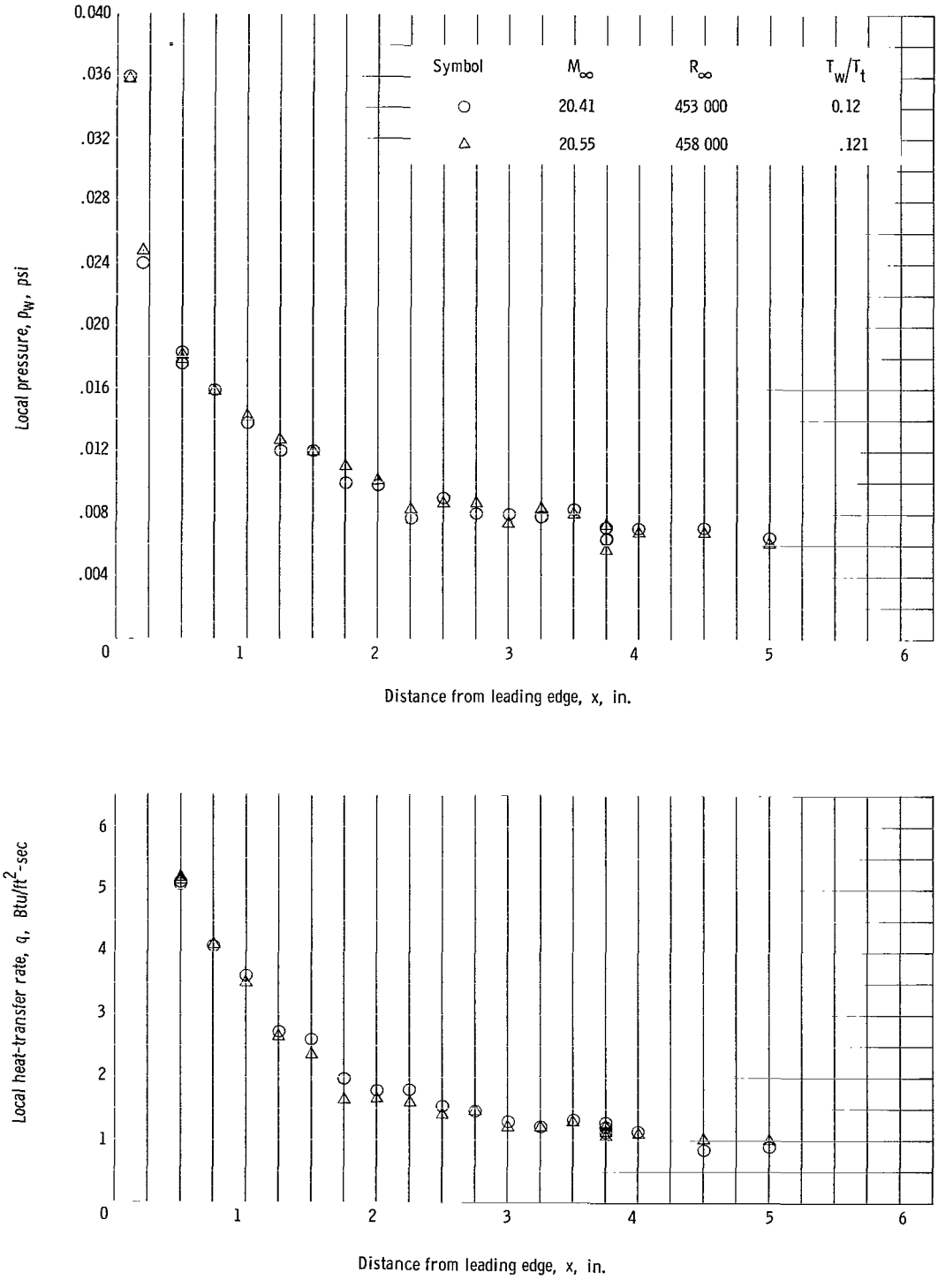

Figure 3.- Typical variation and reproducibility of measured local pressure and heat transfer on sharp flat plate. $\alpha = 0^o$; $\psi = 0^o$; $t_{le} = 0.0003$ in.

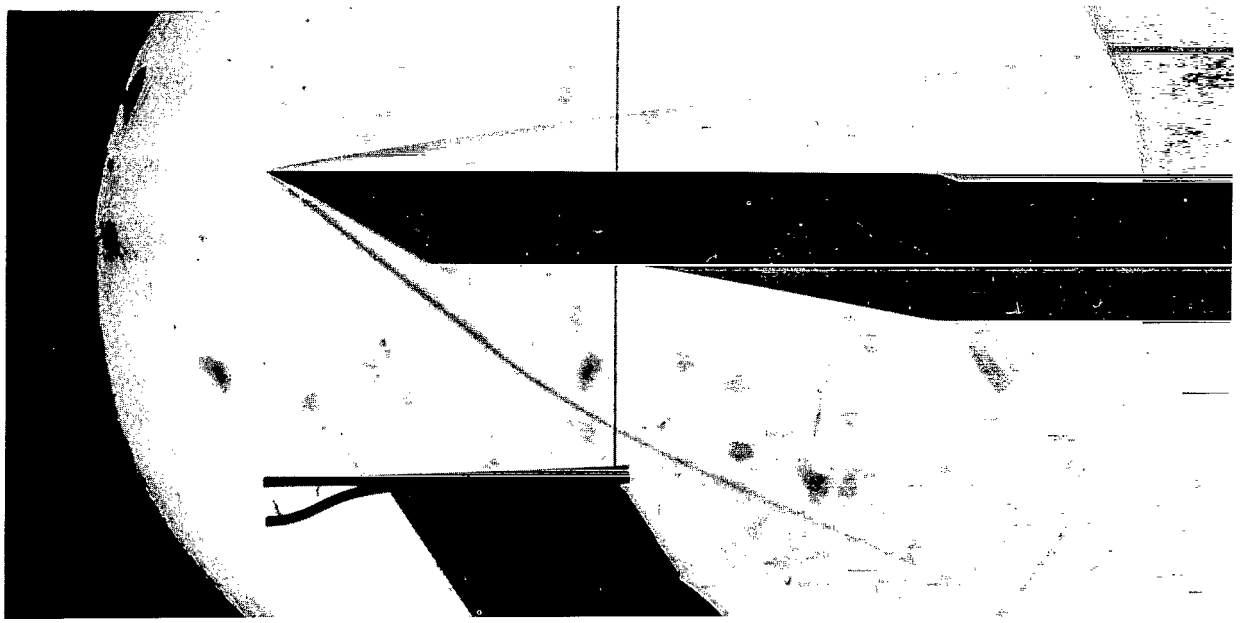

(a) Sharp flat plate; t_{le} = 0.0003 in.

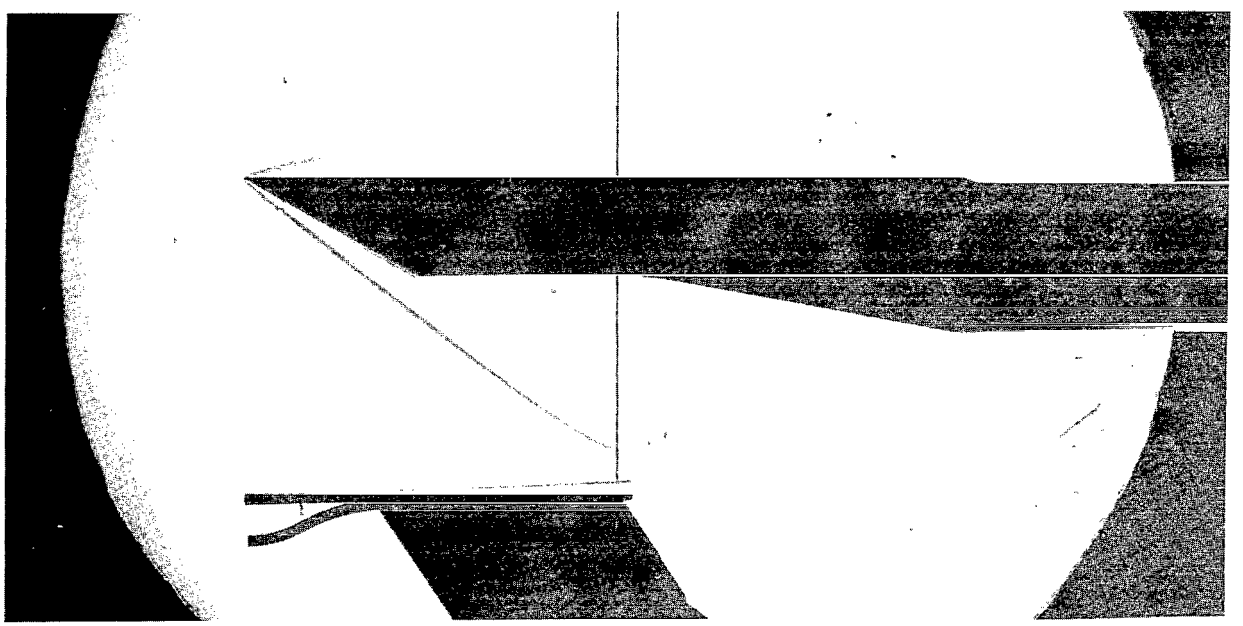

(b) Blunt-nose flat plate; t_{le} = 0.015 in.

L-65-114

Figure 4.- Schlieren photographs of shock shapes on flat plate. $\alpha = 0^{0}$; $T_t \approx 4100^{0}$ R; $M_\infty \approx 20$; $R_\infty \approx 443\,000$/ft.

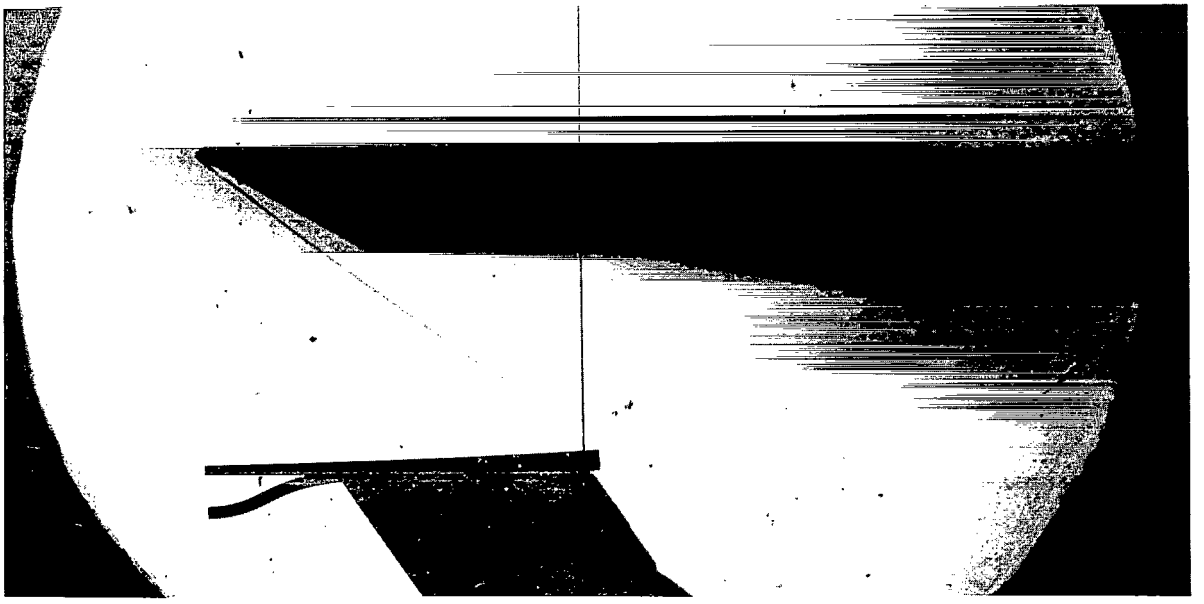

(c) Blunt-nose flat plate; t_{le} = 0.030 in.

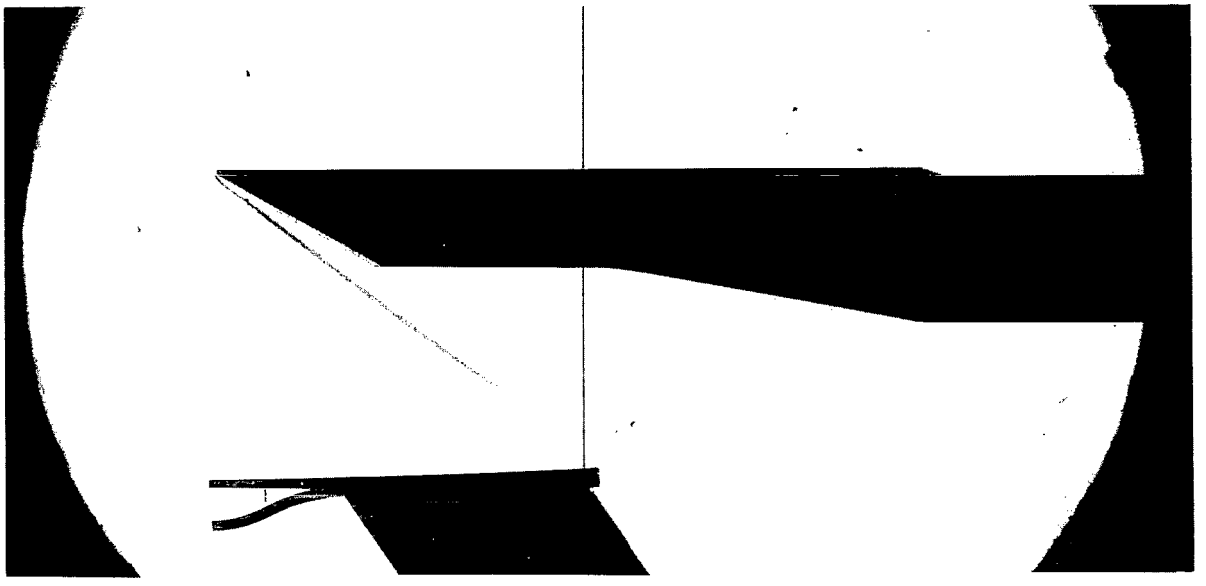

(d) Blunt-nose flat plate; t_{le} = 0.080 in. L-65-115

Figure 4.- Concluded.

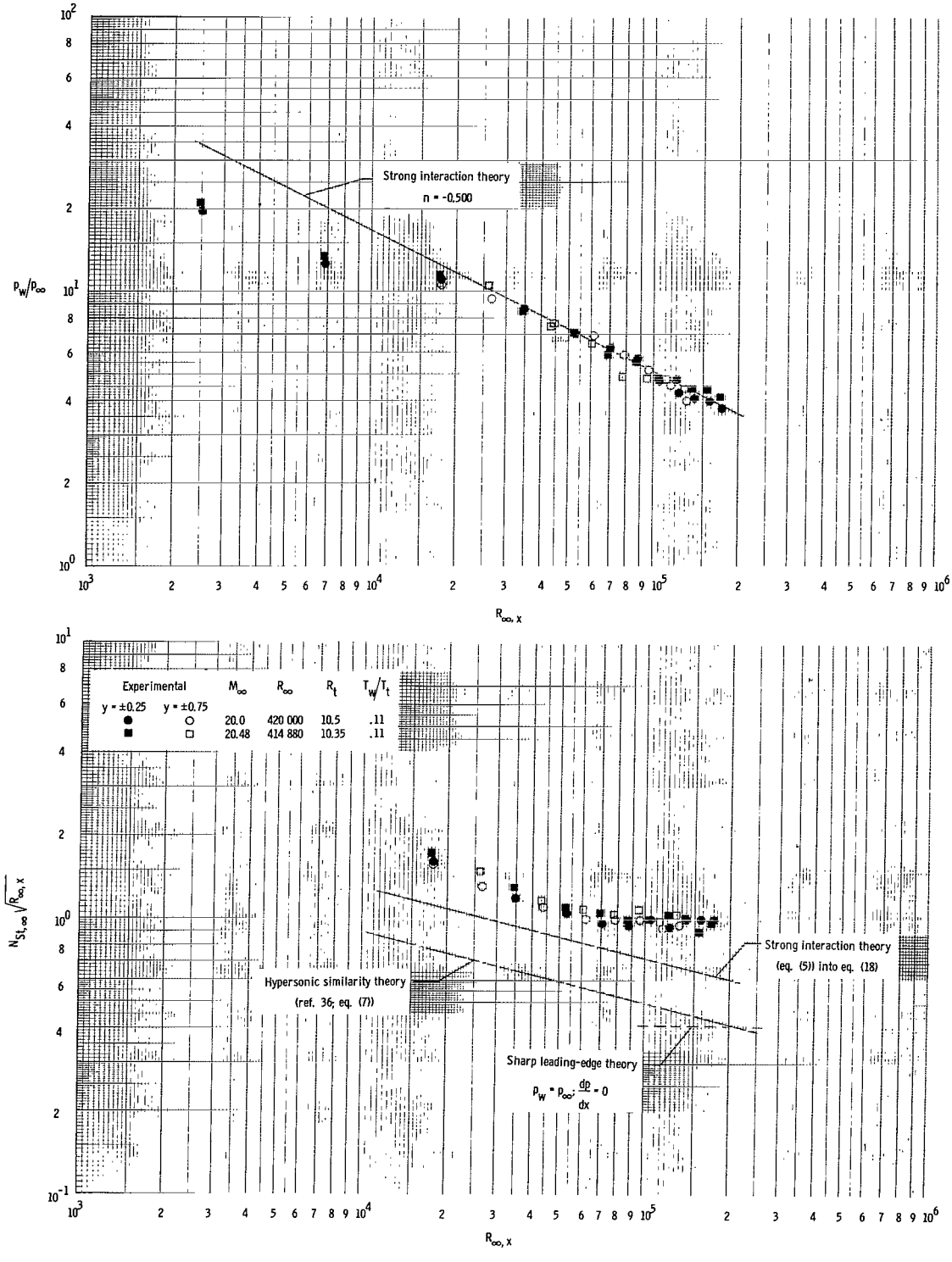

Figure 5.- Pressure and heat-transfer distribution on sharp flat plate. $M_\infty = 20$; $t_{le} = 0.0003$ in.

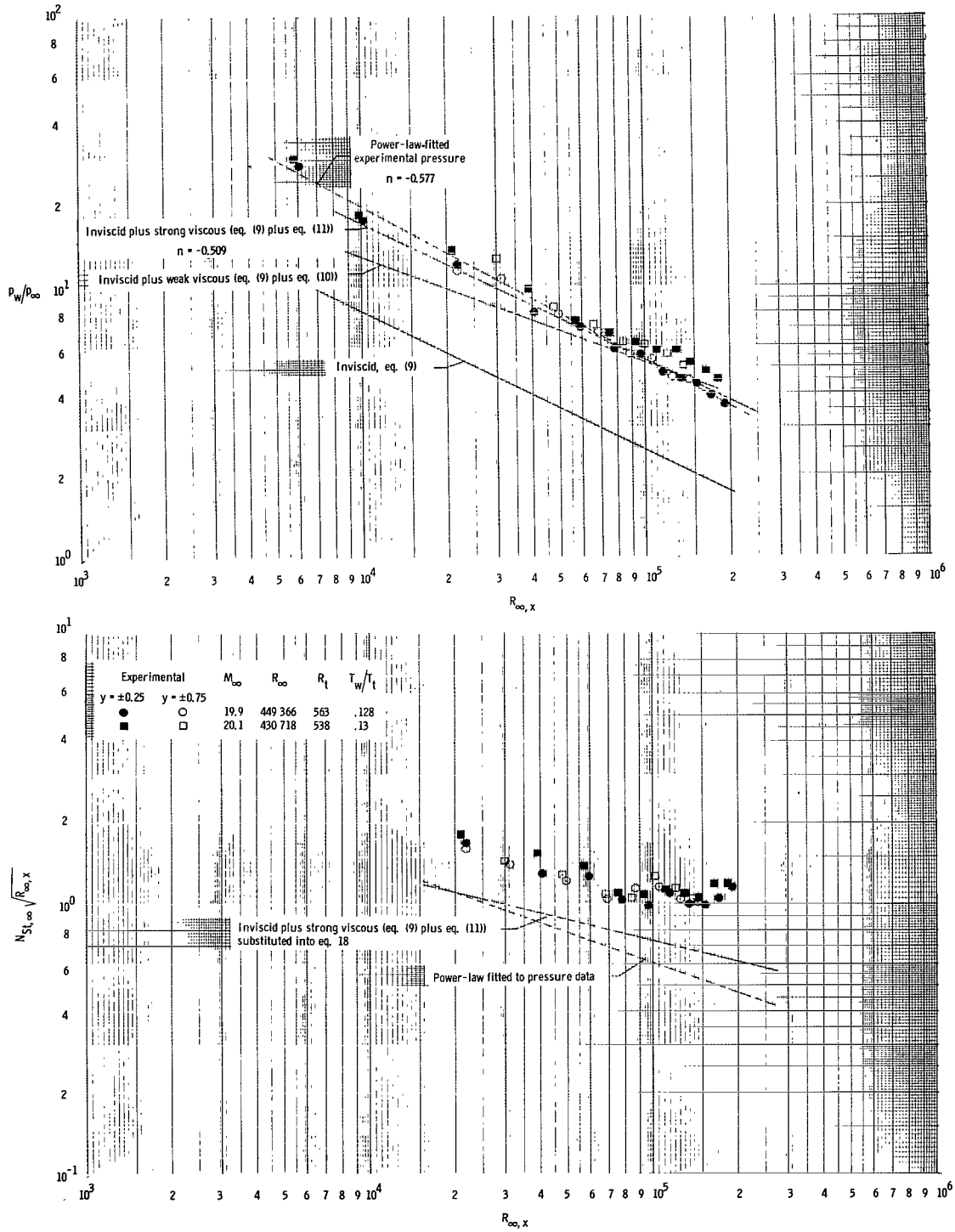

Figure 6.- Pressure and heat-transfer distribution on blunt-nose flat plate. M_∞ = 20; t_{le} = 0.015 in.

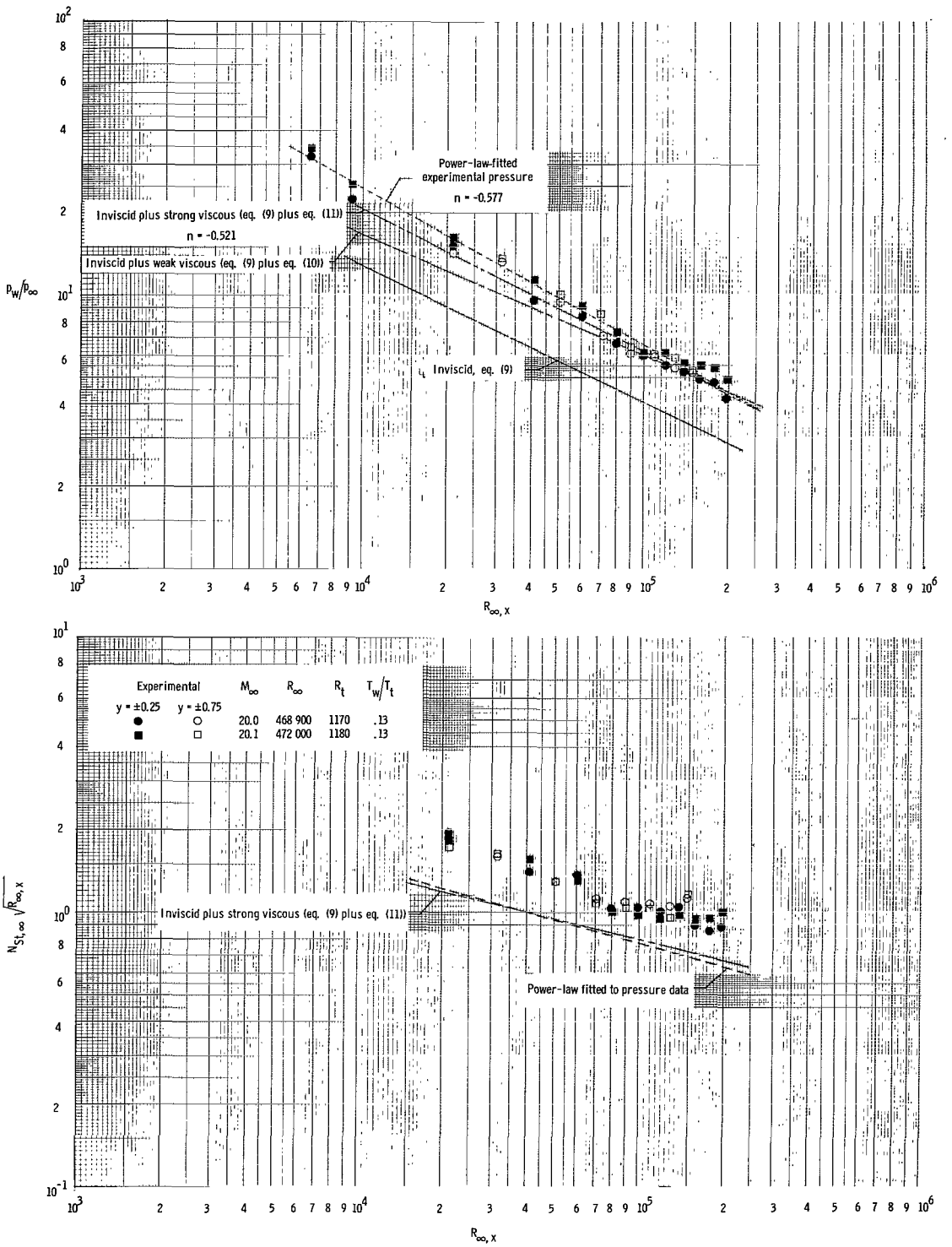

Figure 7.- Pressure and heat-transfer distribution on blunt-nosed flat plate. $M_\infty = 20$; $t_{le} = 0.030$ in.

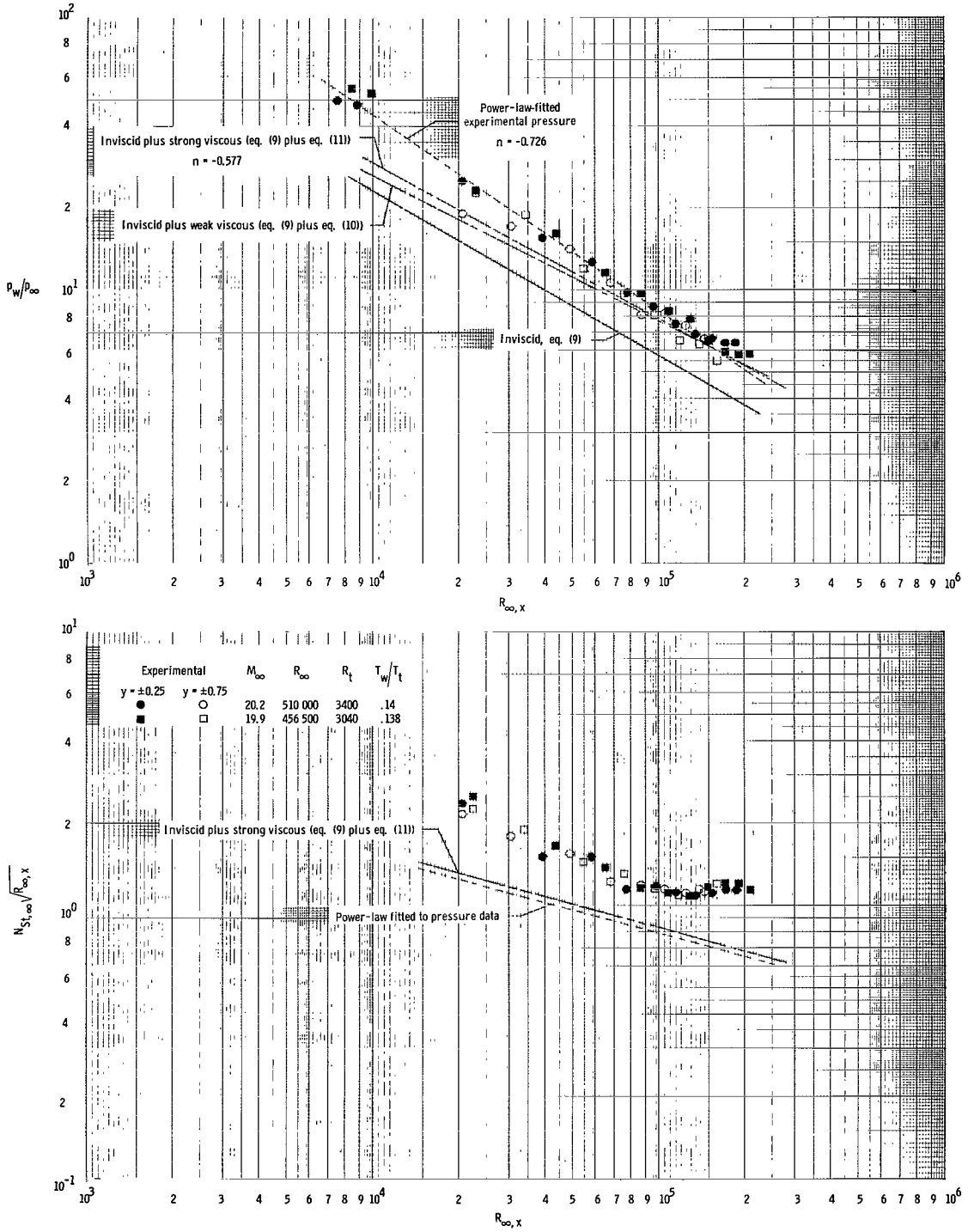

Figure 8.- Pressure and heat-transfer distribution on blunt-nosed flat plate. $M_\infty = 20$; $t_{te} = 0.080$ in.

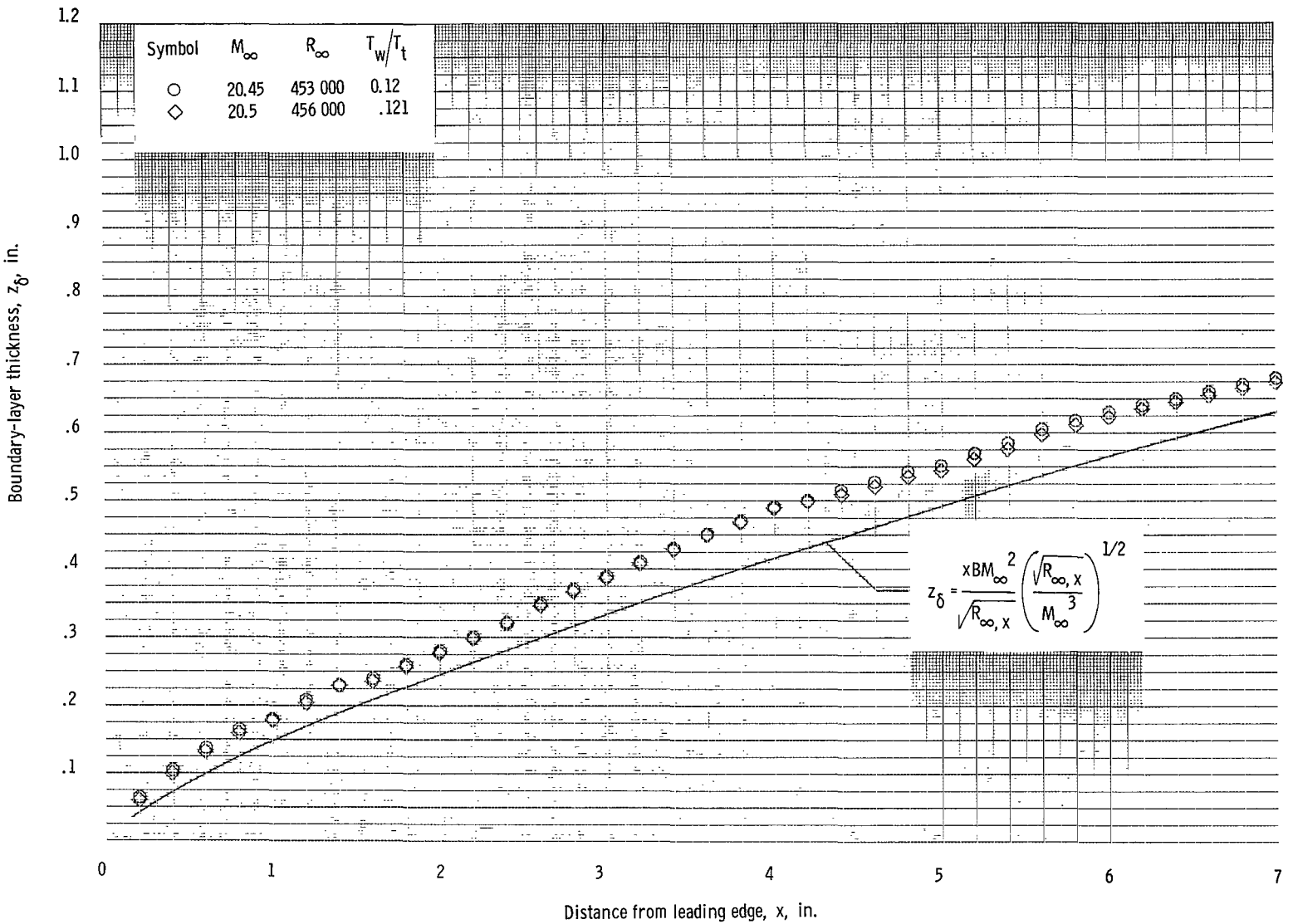

Figure 9.- Boundary-layer thickness on sharp flat plate. t_{te} = 0.0003 in.; $\alpha = 0^0$.

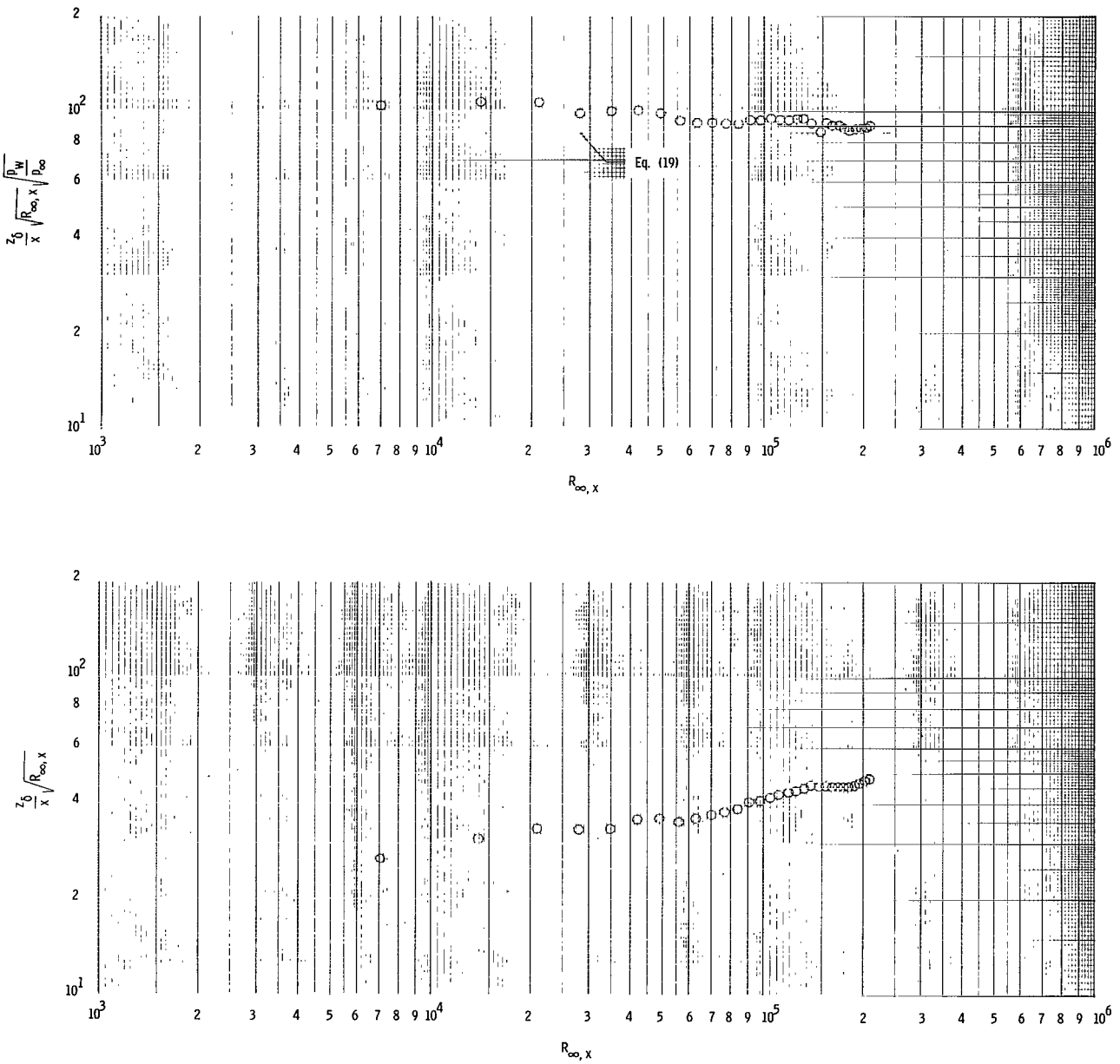

Figure 10.- Effect of local pressure ratio on boundary layer. Sharp-leading-edge flat plate; t_{le} = 0.0003 in.; $\alpha = 0^0$; $M_\infty = 20.45$; $R_\infty = 453\,000$; $T_t = 4100^0$ R.

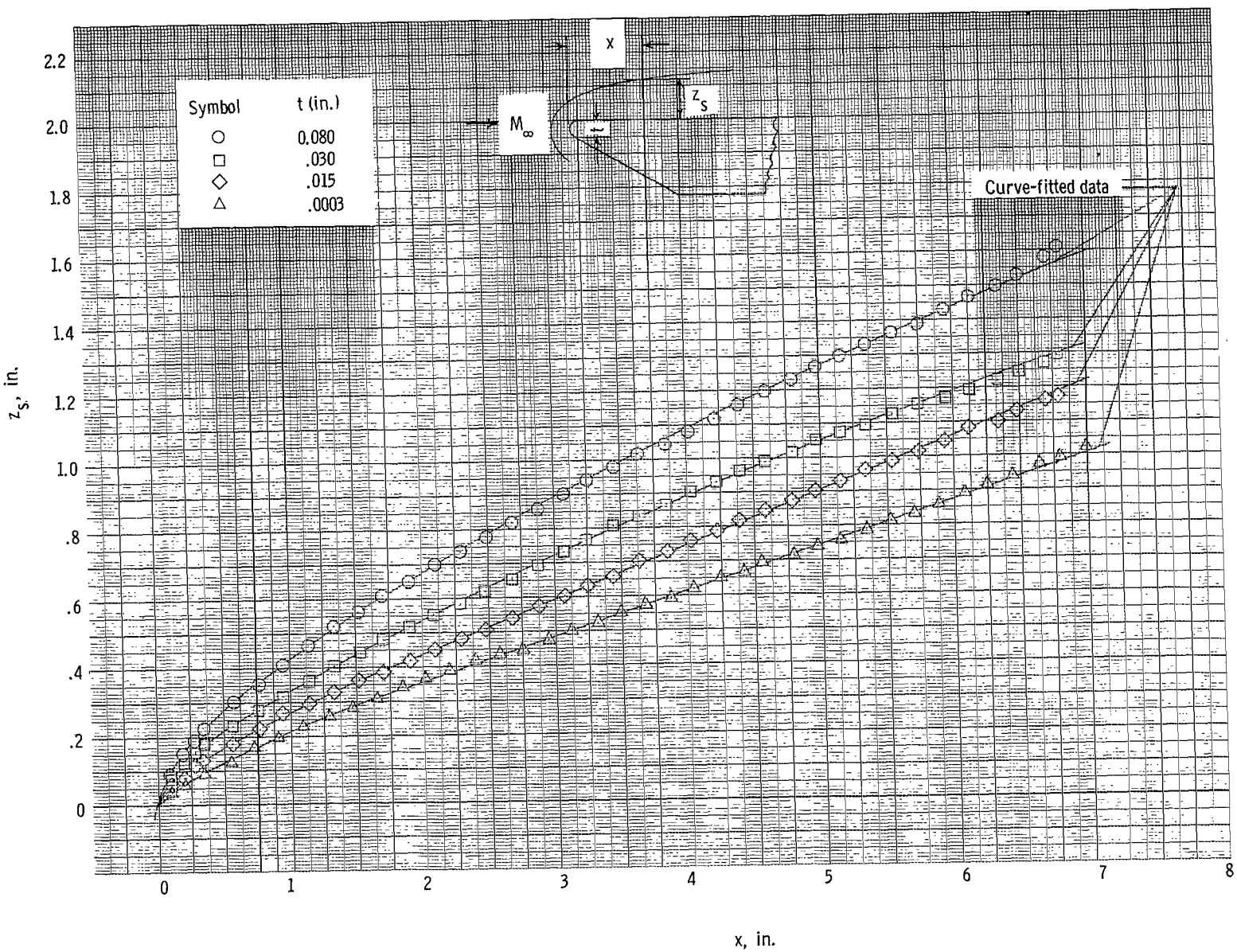

Figure 11.- Summary of shock-wave coordinates. $\alpha = 0^0$; $M_\infty \approx 20$; $T_t \approx 4100^0$ R; $R_\infty \approx 443\,000$/ft.

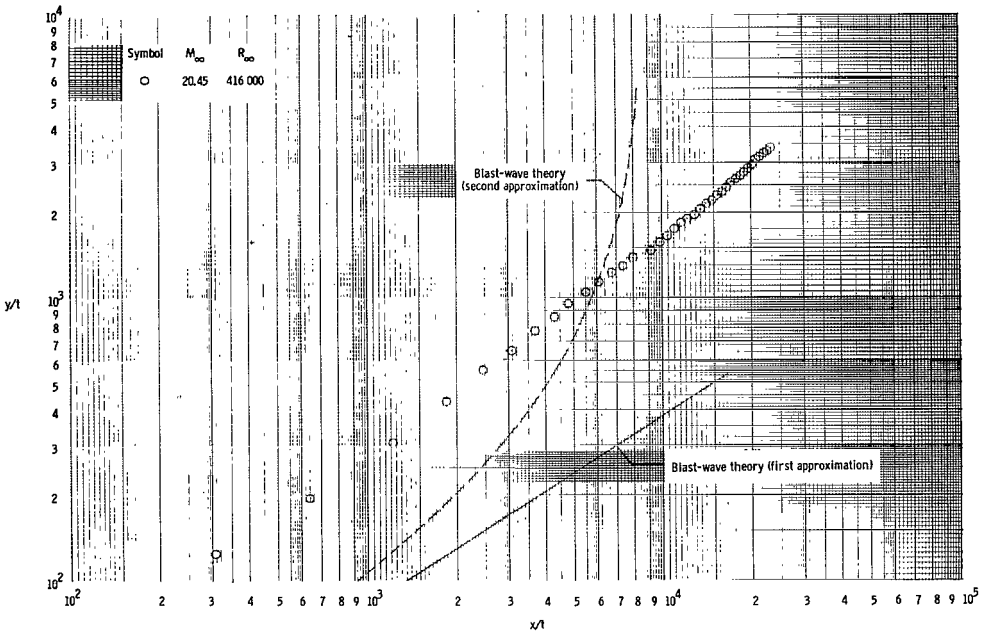

(a) t_{te} = 0.0003 in.

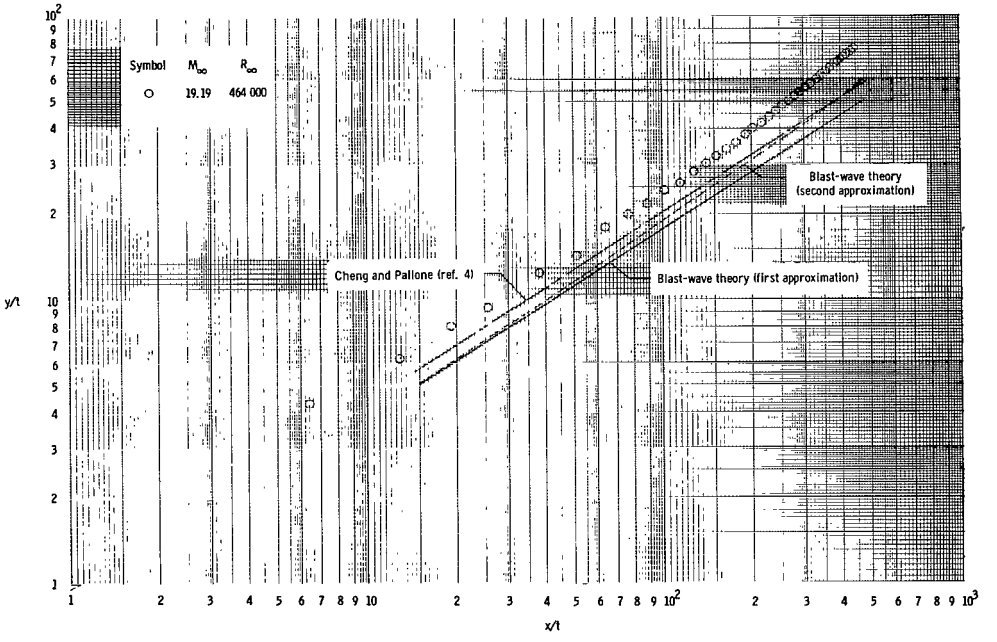

(b) t_{te} = 0.015 in.

Figure 12.- Correlation of shock-wave shapes for $\alpha = 0^0$.

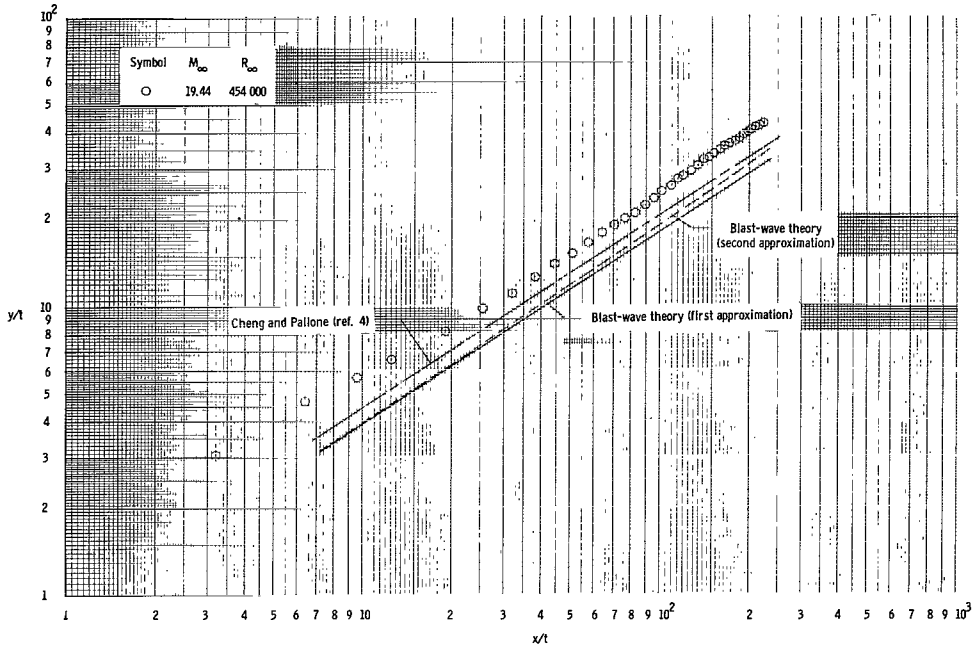

(c) t_{le} = 0.030 in.

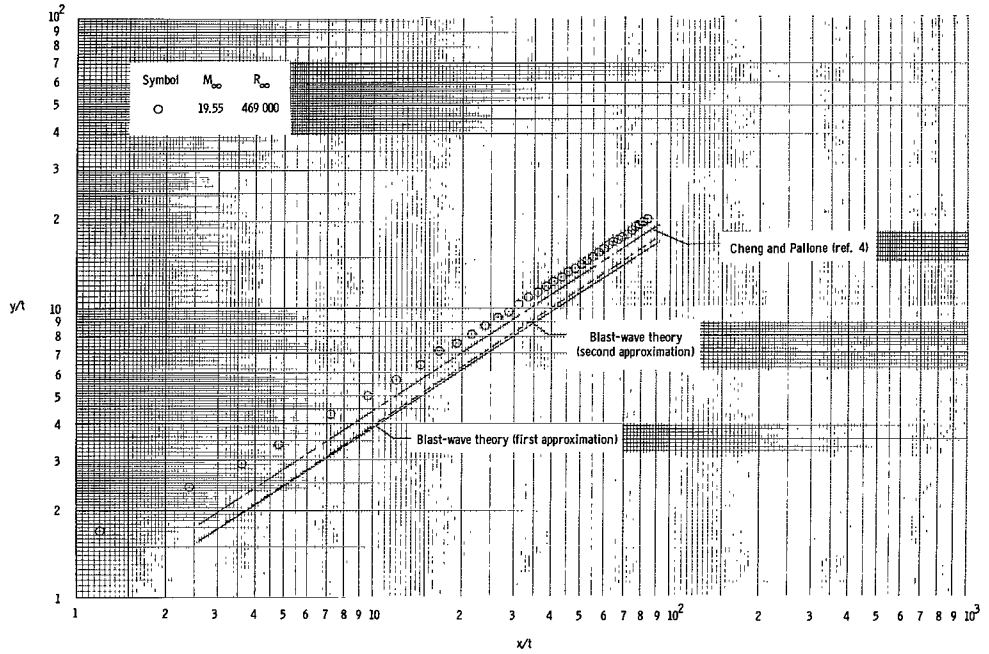

(d) t_{le} = 0.080 in.

Figure 12.- Concluded.

"The aeronautical and space activities of the United States shall be conducted so as to contribute . . . to the expansion of human knowledge of phenomena in the atmosphere and space. The Administration shall provide for the widest practicable and appropriate dissemination of information concerning its activities and the results thereof."

—NATIONAL AERONAUTICS AND SPACE ACT OF 1958

NASA SCIENTIFIC AND TECHNICAL PUBLICATIONS

TECHNICAL REPORTS: Scientific and technical information considered important, complete, and a lasting contribution to existing knowledge.

TECHNICAL NOTES: Information less broad in scope but nevertheless of importance as a contribution to existing knowledge.

TECHNICAL MEMORANDUMS: Information receiving limited distribution because of preliminary data, security classification, or other reasons.

CONTRACTOR REPORTS: Technical information generated in connection with a NASA contract or grant and released under NASA auspices.

TECHNICAL TRANSLATIONS: Information published in a foreign language considered to merit NASA distribution in English.

TECHNICAL REPRINTS: Information derived from NASA activities and initially published in the form of journal articles.

SPECIAL PUBLICATIONS: Information derived from or of value to NASA activities but not necessarily reporting the results of individual NASA-programmed scientific efforts. Publications include conference proceedings, monographs, data compilations, handbooks, sourcebooks, and special bibliographies.

Details on the availability of these publications may be obtained from:

SCIENTIFIC AND TECHNICAL INFORMATION DIVISION

NATIONAL AERONAUTICS AND SPACE ADMINISTRATION

Washington, D.C. 20546